

UNCLASSIFIED

AD 421632

DEFENSE DOCUMENTATION CENTER

FOR

SCIENTIFIC AND TECHNICAL INFORMATION

CAMERON STATION, ALEXANDRIA, VIRGINIA



UNCLASSIFIED

19990211 123

REPRODUCTION QUALITY NOTICE

This document is the best quality available. The copy furnished to DTIC contained pages that may have the following quality problems:

- **Pages smaller or larger than normal.**
- **Pages with background color or light colored printing.**
- **Pages with small type or poor printing; and or**
- **Pages with continuous tone material or color photographs.**

Due to various output media available these conditions may or may not cause poor legibility in the microfiche or hardcopy output you receive.

If this block is checked, the copy furnished to DTIC contained pages with color printing, that when reproduced in Black and White, may change detail of the original copy.

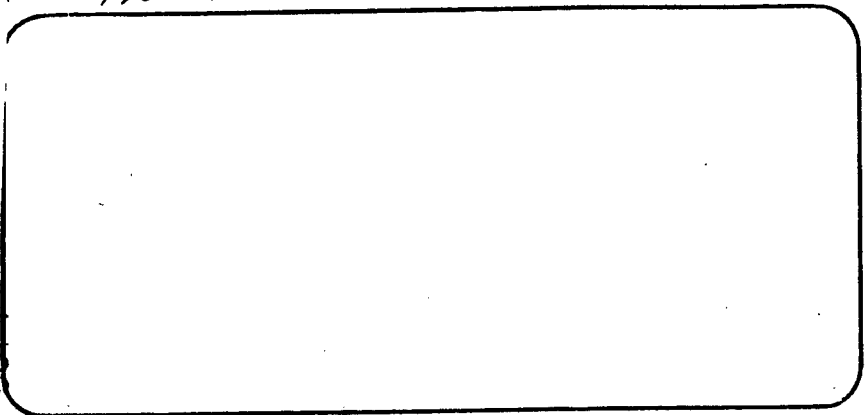
NOTICE: When government or other drawings, specifications or other data are used for any purpose other than in connection with a definitely related government procurement operation, the U. S. Government thereby incurs no responsibility, nor any obligation whatsoever; and the fact that the Government may have formulated, furnished, or in any way supplied the said drawings, specifications, or other data is not to be regarded by implication or otherwise as in any manner licensing the holder or any other person or corporation, or conveying any rights or permission to manufacture, use or sell any patented invention that may in any way be related thereto.

nato

12-1
①

AIR FORCE
TECHNICAL DATA CENTER
TECHNICAL LIBRARY

Document No. 62-09-046
Copy No. 1/2 ONLY



802614

AD No. _____
DDC FILE CL _____

421632



SPACE TECHNOLOGY LABORATORIES, INC.

DDC
RECEIVED
OCT 29 1963
RECEIVED
TISA A

62 09 076

Reproduced From
Best Available Copy

819 500

BSD-TN-61-42

6

SURVEY ON
MISSILE STRUCTURAL DYNAMICS,

10

Prepared by
John D. Wood •

SPACE TECHNOLOGY LABORATORIES, INC.
Los Angeles, California

14 Rept nos. 7102-0041-NU-000 3/1A

EM 11-11

↓

Contract No. AF 64(647)-619

1 June 1961

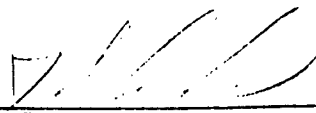
Prepared for

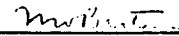
HQ BALLISTIC SYSTEMS DIVISION
AIR FORCE SYSTEMS COMMAND
UNITED STATES AIR FORCE
Air Force Unit Post Office
Los Angeles 45, California
Attention: TDC

62-00-076

Prepared for
HQ BALLISTIC SYSTEMS DIVISION
AIR FORCE SYSTEMS COMMAND, USAF
Under Contract AF 04(647)-619

Prepared 
John D. Wood

Approved 
J. S. Archer
Associate Manager,
Dynamics Department

Approved 
M. V. Barton
Director, Engineering
Mechanics Laboratory

SPACE TECHNOLOGY LABORATORIES, INC.
P. O. Box 95001
Los Angeles 45, California

ACKNOWLEDGEMENT

The author gratefully acknowledges the contributions of those who are listed in the references.

ABSTRACT

ISMAAF
This report is a survey of the more common types of structural dynamics problems in association with ballistic missiles. Special attention is given to the effects of subsystem interaction on dynamic response of the missile and vice versa. A few technically important examples are treated in some detail. The purpose of these examples is twofold; first, they illustrate various techniques used in dynamics analyses and second, they record some of the details of mathematical models which are frequently used to solve missile dynamics response problems. Some of the sections ~~of this report~~ are found in the references, but are repeated here to provide the reader with a fairly complete picture of the more common types of missile structural dynamics problems.

CONTENTS

	Page
1. INTRODUCTION	1
2. IN-FLIGHT DYNAMIC LOADS	4
2.1 Airframe Dynamics -- Lateral Bending	4
2.2 Propellant Dynamics -- Sloshing	10
2.3 Control System	14
2.4 Propulsion System	15
3. SIMPLIFIED EQUATIONS OF MOTION	16
3.1 Missile Deflections	16
3.2 Rigid Body Equations	19
3.3 Missile Bending Equations	22
3.4 Control System and Engine-Swiveling Equations	23
3.5 Block Diagrams	27
3.6 Use of Equations	29
4. ILLUSTRATIVE EXAMPLES	33
4.1 Limit Cycle Response	33
4.2 Response Due to Gust	34
5. PRELAUNCH--POSTLAUNCH DYNAMIC LOADS	38
5.1 Wind-Induced Oscillations	38
5.1.1 Theoretical Considerations	38
5.1.2 An Example	48
5.2 Launching in a Wind	49
5.2.1 Solution of the Problem	49
5.2.2 An Example	53
5.3 Effects of Thrust Build-up	57
5.3.1 Theoretical Considerations	57
5.3.2 An Example	63
5.4 Missile Response Due to Ground Shock	65
APPENDIX	
MODELS FOR THE LONGITUDINAL VIBRATIONS OF LIQUID PROPELLANT TANKS	74
REFERENCES	86

ILLUSTRATIONS

Figure	Page
1. Dynamical Environments	3
2. Element of a Timoshenko Beam	5
3. Typical Free-Free Missile Bending Modes	11
4. Influence of Shear Deflection, Rotatory Inertia, and Axial Acceleration on Bending Frequencies.	12
5. Fluid Sloshing	13
6. Geometry and Coordinate System	17
7. Forces Acting on Missile.	20
8. Schematic of Autopilot Actuator	24
9. Block Diagram of Autopilot and Engine Dynamics.	26
10. Block Diagram Showing Detailed In-Flight Interactions.	28
11. Functional Block Diagram	30
12. Dynamic Loads Generated by a Control System Limit Cycle.	33
13. Bending Coordinates During Δ Gust	35
14. Inflight Response Due to Δ Gust.	36
15. Missile Exposed to Ground Winds	39
16. Normalized Power Spectrum for the Lift Force and Drag Force at Reynolds Number 1.39×10^6	42
17. Bending Moments on a Typical Missile Exposed to a Uniform 60-mph Wind.	49
18. Coordinate System of Constrained Missile	51
19. Absolute Maximum Bending Moments at Launch.	54
20. Absolute Sum of Peak Mode Responses of Bending Moments Due to Sudden Release from Initial Deflection.	56
21. Inboard Profile and Mass-Spring Analog of Missile	58
22. Effect of Damping and Release Time on Missile Axial Loads Due to Launch and Engine Thrust Transients	64
23. Engine Thrust Build-up Curve	64

ILLUSTRATIONS (Continued)

Figure	Page
24. Missile-Launcher	67
25. Response of Single Degree of Freedom System to Ground Motion	71
26. Horizontal Displacement Shock Spectrum	72
27. Propellant Tank	74
28. Displacement of Fluid Due to Tank Wall Expansion.	78
29. Longitudinal Model of Propellant Tank	78
30. Longitudinal Model of Propellant Tank With Flexible Lower Bulkhead	80
31. Section of Skin-Stringer Cylinder and Longitudinal Model	82
32. Longitudinal Model of Semi-Monocoque Cylinder With Partially Buckled Skin	84
33. Simplified Model of Figure 32.	85

I. INTRODUCTION

The need for a current survey and reference document on the more common missile structural dynamic problems and their analyses resulted in the writing of this report. Many of the sections of the report appear in previous works, as referenced, however they have been revised and repeated here to provide an overall picture of the necessity and complexity in studying missile dynamic response problems.

The assumption of a rigid structure is necessary in the preliminary design phase of a missile in order to allow the computation of loads on which further design work can be based. However, once a preliminary structural design has been made it is possible to compute the dynamic characteristics of the missile. Utilizing these dynamic characteristics, dynamic loads, * a revision to the initial load estimates, can be determined.

In this report the problem of determining dynamic loads will be discussed. Special attention will be given to the effects of subsystem interaction on dynamic loads and vice versa. A few technically important examples will be treated in some detail.

For purposes of the discussion which follows, a complete missile system is envisioned as being composed of the following subsystems: (A) airframe (structure) including propellants, (B) propulsion system, (C) control system, (D) payload (re-entry vehicle, satellite, etc.), (E) launch facilities. Each of these subsystems has its own peculiar dynamic characteristics which, from the dynamic loads point of view,

* Throughout this report the term "dynamic load" is used to designate those stresses, bending moments, shear forces, etc., which are generated by a time-dependent environment. The stresses, etc., are, of course, functions of time.

are not exceptionally interesting. However, once these subsystems are interconnected, the picture may change completely. For example, a propulsion system generates a thrust which builds from zero to a more or less steady value and then later decays to zero. The time-dependent character of the thrust produces no startling behavior when acting on a rigid airframe; the situation can be dramatically different when the dynamic behavior of the airframe is considered. These types of dynamic interactions and their effect on dynamic loads are the central theme of what follows. Some of the dynamical environments which are considered to effect the missile response are illustrated in Figure 1. The effects of dynamical environments shown in Figure 1 which are not considered in this report such as unsteady aerodynamics (buffeting) and microseisms are given in References 1 to 3.

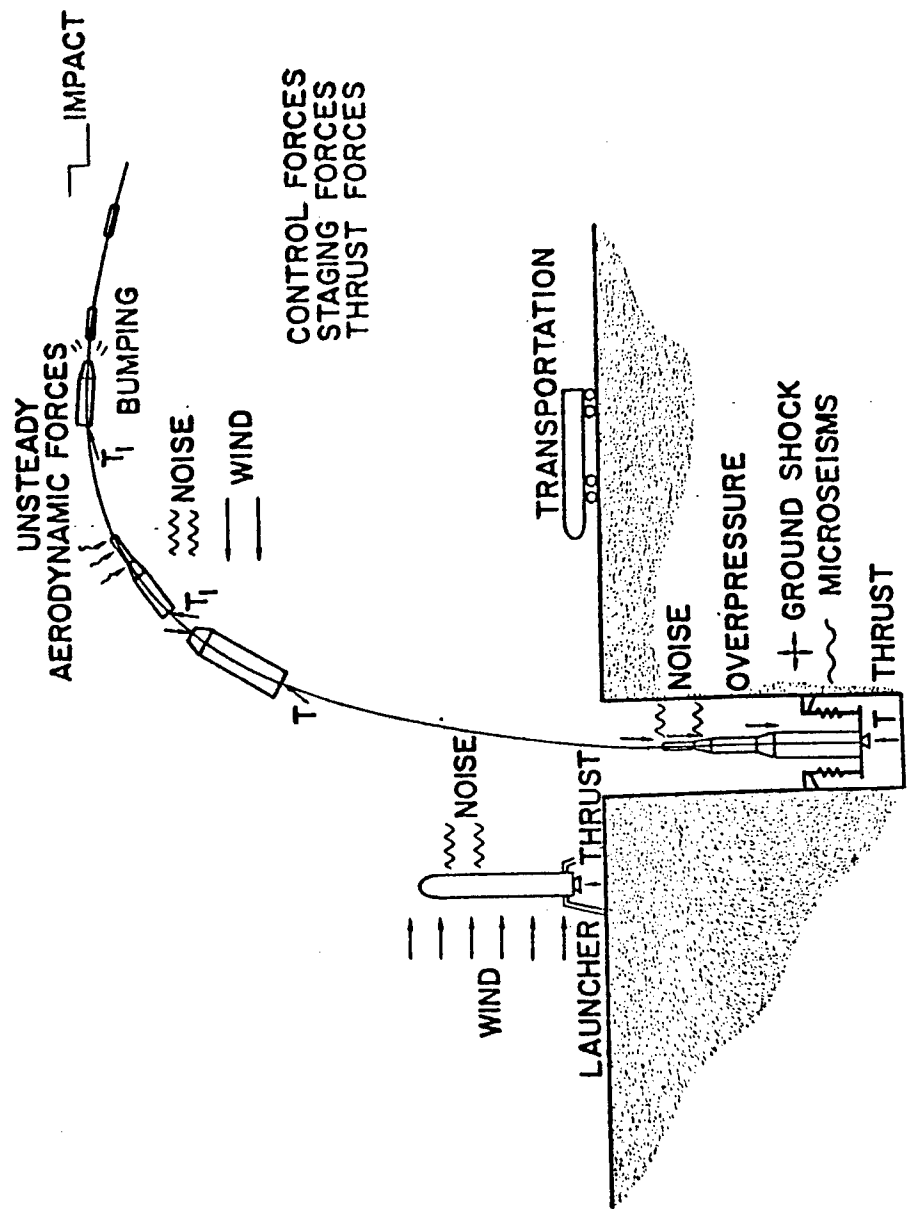


Figure 1. Dynamical Environments

2. IN-FLIGHT DYNAMIC LOADS

In this section equations for the lateral motion of a liquid propellant missile will be developed. These equations, which include aerodynamic forces, control system dynamics, airframe dynamics, and propellant dynamics, can be used to compute dynamic loads for a variety of inputs. In addition, they can also be used to study control system stability. These equations are evolved in References 4 through 12.

2.1 Airframe Dynamics - Lateral Bending

Experimental studies have established the fact that a missile airframe can be idealized as a nonuniform (in stiffness and mass distribution) beam for purposes of studying its lateral bending dynamics. Sometimes it may be necessary to represent an airframe as a collection of beams rather than as a single beam. However, such a representation poses no theoretical difficulties, although computational problems may develop.

It has been established, both theoretically and experimentally, that simple (Bernoulli-Euler) beam theory does not accurately represent bending dynamics of airframes of the dimensions encountered in ballistic missiles. An adequate bending theory must account for the effects of shear deformation and, usually, the rotational inertia of beam elements. Such a theory, known as the Timoshenko beam theory, is available.

The Timoshenko equations are derived by writing the equilibrium and kinematic equations for a differential element of the beam as shown in Figure 2. The beam has a number of spring-mass systems attached at distances l_j from the mass center. The reasons for including these systems will become clear later. Equilibrium of the lateral forces acting on the element requires that (see References 5, 11 and 12)

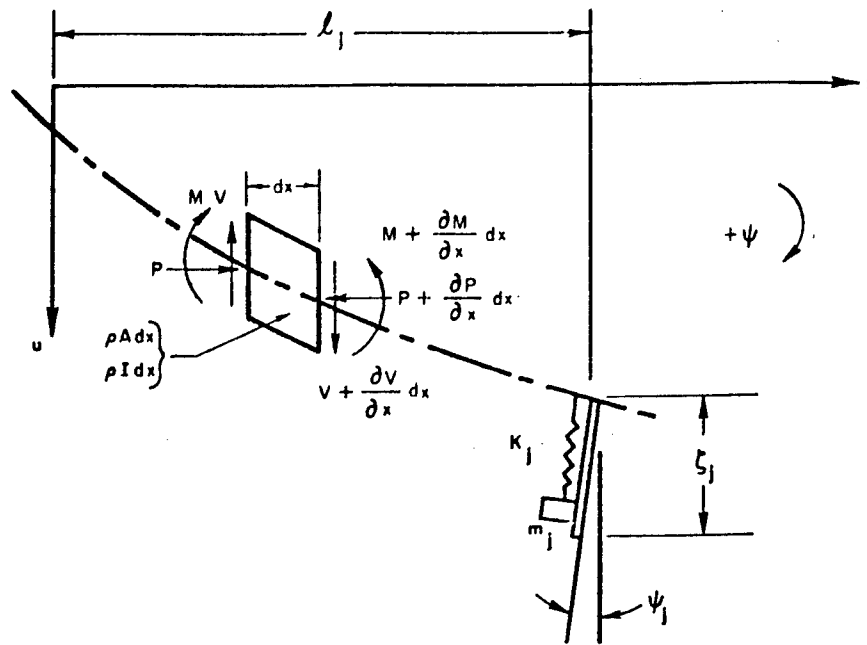


Figure 2. Element of a Timoshenko Beam

$$\rho A \ddot{u} = \frac{\partial V}{\partial x} + \sum_{j=1}^N \Delta(x - l_j) (K_j \zeta_j + m_j a_x \psi_j) \quad (1)$$

Writing equilibrium of moments and dropping second-order terms gives

$$\rho I \ddot{\psi} = -\frac{\partial M}{\partial x} + V + P \frac{\partial u}{\partial x} - \sum_{j=1}^N \Delta(x - l_j) a_x m_j \zeta_j \quad (2)$$

where $\Delta(x - l_j)$ is the Dirac delta function defined by

$$\begin{aligned} \Delta(x - l_j) &= 0 && \text{when } x \neq l_j \\ \int_{l_j - \epsilon}^{l_j + \epsilon} \Delta(x - l_j) dx &= 1 && \text{as } \epsilon \rightarrow 0 \end{aligned} \quad (3)$$

and where

u = total deflection of beam, due to both bending and shear

ψ = slope of beam due to bending alone

ζ_j = displacement of j th attached spring-mass system relative to deflected position of beam

ρA = the mass per unit length

V = the shear force on a cross section

ρI = the mass moment of inertia per unit length of the beam cross sections

M = the bending moment on a cross section

P = the axial load in the beam at any section

$$= -a_x \int_x^{\text{tip}} \rho A dx - a_x \sum_{j=1}^{N_1} m_j$$

a_x = absolute acceleration of beam system in negative x -direction

N_1 = number of slosh masses between x and tip.

Only the rotary inertia forces caused by the bending slope appear in Equation 2. The shear forces produce distortion only and not rotation of the beam elements. The moment curvature relationship for a Timoshenko beam is the same as for a simple beam, namely

$$EI \frac{\partial \psi}{\partial x} = -M \quad (4)$$

where EI is the flexural rigidity of the beam. Because of the inclusion of shear deformation, another equation, describing the relationship of shearing forces to shearing deformations, is required. This relation is

$$KAG \left(\frac{\partial u}{\partial x} - \psi \right) = V + P \frac{\partial u}{\partial x} \quad (5)$$

where KAG is the shear rigidity of the beam, and $\partial u/\partial x - \psi$ is the shearing slope. Incorporating Equations 4 and 5 into the equilibrium Equations 1 and 2 yields the following Timoshenko beam equations (see References 5, 11, and 12):

$$\rho A \ddot{u} = \frac{\partial}{\partial x} \left[KAG \left(\frac{\partial u}{\partial x} - \psi \right) - P \frac{\partial u}{\partial x} \right] + \sum_{j=1}^N \Delta(x - \ell_j) (K_j \zeta_j + m_j a_x \psi_j)$$

$$\rho I \ddot{\psi} = \frac{\partial}{\partial x} \left[EI \frac{\partial \psi}{\partial x} \right] + KAG \left(\frac{\partial u}{\partial x} - \psi \right) - a_x \sum_{j=1}^N \Delta(x - \ell_j) m_j \zeta_j \quad (6)$$

A simplified form of these equations can be found in many standard texts on the vibrations of continuous systems (see, for example, Reference 13). The provisions for attached springs and masses and the inclusion of the axial compression force $P = P(x)$ are not usually given explicitly in these texts. Inclusion of the axial compression force in the equations is sometimes important in missile applications because the axial acceleration of the missile in flight can affect the bending dynamics.

At this point it is useful to review briefly what is meant by normal modes and describe some of their properties. If an external force acting on the missile varies sinusoidally at a single frequency, and this frequency is slowly varied, we would observe a series of resonances at a number of discrete frequencies. At these frequencies, the amplitude of vibration becomes quite large, and each point of the missile reaches its maximum displacement at the same time, describing a definite pattern in space. This pattern or mode shape is commonly called an eigenfunction or normal mode (given by $\phi_n(x)$, $\psi_n(x)$ here), and the frequency at which it occurs is called an eigenvalue. A very important property of these modes is that the motion of the missile in any one mode is independent of the motion taking place in any of the others, except through

coupling from external forces (see later). This is due to the orthogonality property of the normal modes, and because of this independence it is usually expedient to describe the missile motion in terms of these modes.

The mathematical expressions which describe the orthogonality of the normal modes can be obtained directly from the differential equations of motion. The derivation of these orthogonality conditions is straightforward and follows the standard procedure given in many texts. The orthogonality conditions for Equation 6 are; (see Reference 11)

$$\int_l (\rho A \phi_m \phi_n + \rho I \psi_m \psi_n) dx + \sum_{j=1}^N m_j (\phi_{jm} + \zeta_{jm}) (\phi_{jn} + \zeta_{jn}) = \begin{cases} M_n, & m = n \\ 0, & m \neq n \end{cases}$$

$$\int_l EI \frac{d\phi_m}{dx} \frac{d\phi_n}{dx} dx + \int_l KAG \left(\frac{d\phi_m}{dx} - \psi_m \right) \left(\frac{d\phi_n}{dx} - \psi_n \right) dx$$

$$- \int_l P \frac{d\phi_m}{dx} \frac{d\phi_n}{dx} dx + \sum_{j=1}^N K_j \zeta_{jm} \zeta_{jn}$$

$$+ a_x \sum_{j=1}^N m_j (\psi_{jm} \zeta_{jn} + \psi_{jn} \zeta_{jm}) = \begin{cases} M_n \omega_n^2, & m = n \\ 0, & m \neq n \end{cases} \quad (7)$$

where

ϕ_n is the eigenfunction for deflection, and

ψ_n is the eigenfunction for bending slope

and $\phi_{jm} \equiv \phi_m(x)|_{x=l_j}$, that is, $\phi_m(x)$ evaluated at $x = l_j$, and ζ_{jm} is the displacement of the j th mass in the m th mode, and the subscripts m and n refer to two different modes. The constant M_n is the generalized mass of the n th mode, ω_n is its circular frequency, and a_x is the axial acceleration of the missile. If we denote the amplitude of the n th mode at any instant of time by $q_n(t)$, these amplitudes can be used as generalized coordinates.

Setting up the kinetic and potential energies in terms of these $q_n(t)$, and using orthogonality conditions 7, the equations of motion for the $q_n(t)$ can be reduced to the following form: (see Reference 12 for more detail)

$$\begin{aligned}
 M_n \ddot{q}_n(t) + M_n 2b_n \omega_n \dot{q}_n + M_n \omega_n^2 q_n(t) &= Q_n(t) - \delta \int_0^b \left[z(\rho \Lambda_e) \phi_n - (\rho I_e) \psi_n \right] dz \\
 &- K_{2n} \left[\ddot{\theta} + K_1 (\dot{\delta} + \delta \omega_n^2) \right] \\
 &- m_e \bar{z}(a_x) \delta \phi_n'(-l_e) \\
 &\triangleq Q_n(t) + \bar{Q}_n(t) \tag{8}
 \end{aligned}$$

where $Q_n(t)$ is the generalized force acting on the n th mode. This force can be found in the usual way by giving the n th mode a virtual displacement Δq_n and finding the work done by all the external forces acting on the missile. The presence of only one mode amplitude q_n in Equation 8 demonstrates the usefulness of the bending modes being independent of each other. K_1 and K_{2n} are defined later.

To return to the problem at hand, Equation(6) can be solved, subject to appropriate boundary conditions, to yield a set of bending modes $\phi_n(x)$, $\psi_n(x)$.^{*} For the missile in-flight, the ends of the missile are free, and the engine can be treated as an integral part of the beam, clamped with zero control angle δ ; disconnected from the missile altogether; or attached to the missile by some intermediate constraint. The resulting equations, showing the interaction between the bending and the control system, differ slightly depending on what representation of engine attachment is made for the computation of the bending modes. The equations that follow assume the modes to have been computed with the engine clamped at $\delta = 0$.

*Some practical procedures for computing the bending modes are discussed in References 8 and 16.

Typical free-free missile bending modes and frequencies for various flight times are shown in Figure 3. It is noted that the first free-free mode frequency varies by less than 10 percent in the flight time interval from launch to 100 seconds.

The influence of shear deformations, rotatory inertia, and axial acceleration on the missile bending frequencies is shown in Figure 4. In the first mode the inclusion of shear deflection, noted as $KAG = n$ and the exclusion of rotatory inertia noted as $\rho I = 0$ increases the frequency by 0.5 percent over the frequency if both effects are included. Note that the exclusion of shear deformation changes the first mode frequency by 12.1 percent. If axial acceleration is omitted in the bending mode analyses, the first mode frequency is increased by 27 percent and one percent for constrained (prelaunch) and free flight conditions respectively.

2.2 Propellant Dynamics—Sloshing

The description of the missile dynamics for missiles with liquid propellants is complicated by the interaction between the airframe and the propellants. As the missile bends and rotates, the liquid propellants move back and forth in their tanks as shown in Figure 5, creating very appreciable forces on the missile.

It can be shown that only the fundamental (lowest frequency) mode of propellant motion contributes significantly to these forces. The fundamental mode of motion, depicted in Figure 5 is called the "sloshing" mode. The resonant frequencies of these sloshing modes are usually quite low (approximately 0.5 cps) and they interact severely with the autopilot. Furthermore, since the sloshing frequencies are considerably below the first free-free "bending" frequency of the missile structure, the external airframe rotates back and forth, essentially as a rigid body in some of the "sloshing" modes, in a direction opposite from the fluid sloshing in order to preserve angular momentum. This means that the interaction between sloshing and aerodynamics is also rather

TYPICAL FREE-FREE MISSILE BENDING MODES

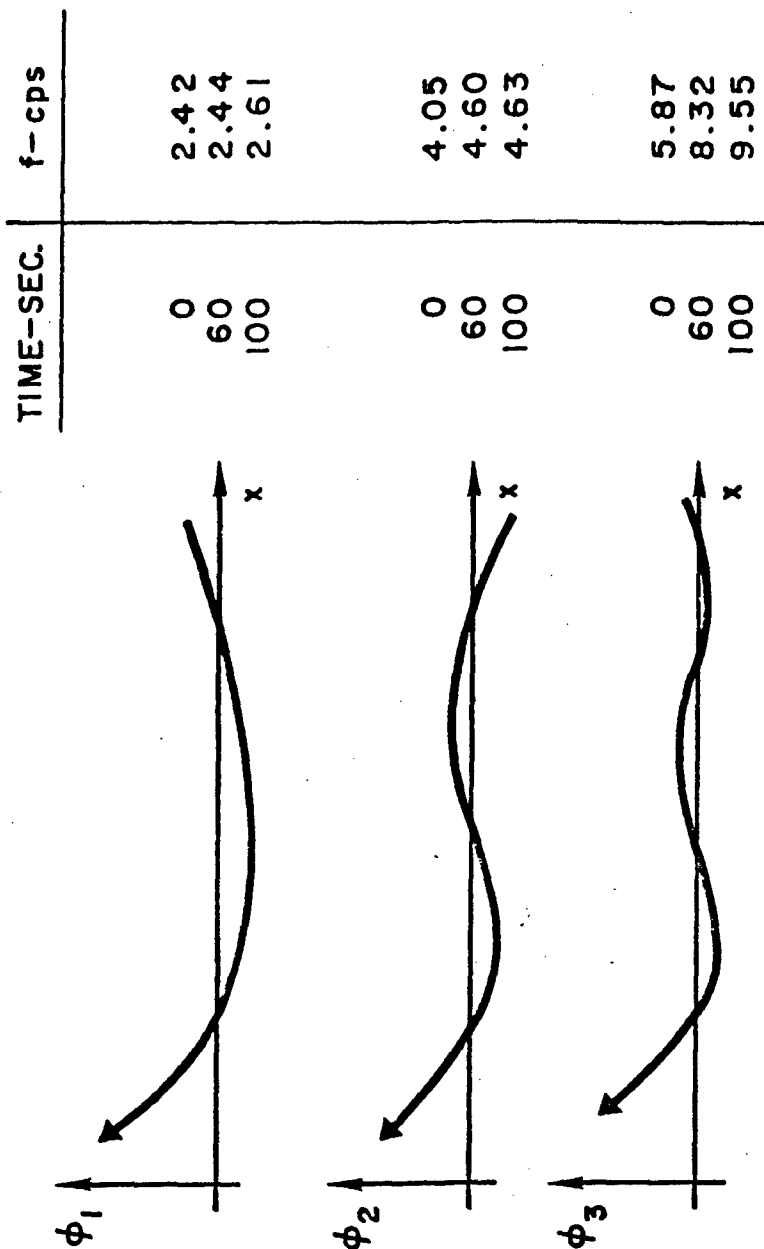


Figure 3. Typical Free-Free Missile Bending Modes

INFLUENCE OF SHEAR DEFLECTION,
ROTATORY INERTIA, AND AXIAL
ACCELERATION ON BENDING FREQUENCIES

MODE NO.	KAG	ρI	f/f_n	MISSILE ON LAUNCHER
1	n	0	1.005	$f_0 / f_a = 1.27$
	∞	n	1.121	
2	n	0	1.011	MISSILE IN FLIGHT
	∞	n	1.350	
3	n	0	1.013	$f_0 / f_a = 1.01$
	∞	n	1.538	

Figure 4. Influence of Shear Deflection, Rotatory Inertia, and Axial Acceleration on Bending Frequencies

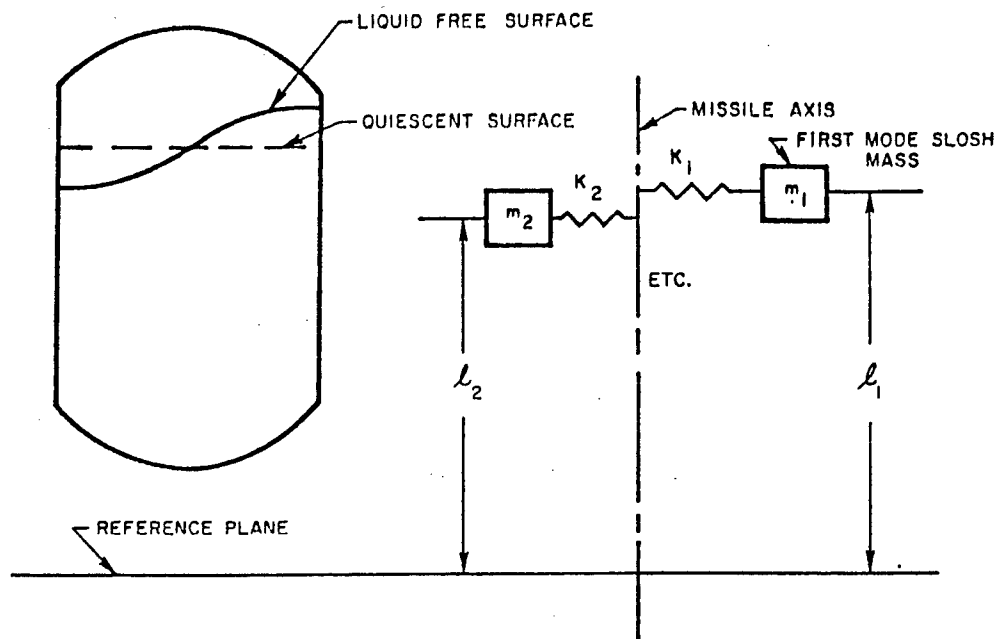


Figure 5. Fluid Sloshing

strong since the entire missile picks up an angle of attack during the sloshing motion. The interaction between aerodynamic forces and those missile modes that consist mainly of structural bending is not nearly as strong; only a local angle of attack is generated, and the resulting aerodynamic forces are usually negligible.

One possible scheme for eliminating the sloshing problem would be to divide the propellant tanks into small compartments, thereby increasing the slosh frequencies and reducing the sloshing forces. Unfortunately, because of weight considerations, such a procedure is generally highly impractical. However, small ring baffles are usually placed at various levels in the tanks. These baffles do not change the sloshing frequencies but do provide natural damping by creating turbulence in the regions of high liquid velocity.

The separate airframe and propellant dynamics may be combined to yield what are known as bending-sloshing modes. To obtain these combined modes, the fluid is treated as concentrated along the missile center line, and the sloshing modes in each tank are represented by attached springs and masses. The spring-mass systems are selected to give the correct slosh frequencies and horizontal force, and their attachment points are selected to give the same moments about the tank center of gravity as is produced by the fluid. The rotatory inertia assigned to the fluid, ρI in Equation 6, is adjusted so that the overall inertia of the fluid in each tank is the same as that found by solving the fluid dynamics problem of a tank capped at the quiescent liquid surface. Equation 6, when coupled with appropriate equations defining K_j , will yield combined bending-sloshing natural frequencies and mode shapes. Those readers who wish to pursue the propellant dynamics problem further will find a discussion of the sloshing problem in References 7 and 14.

2.3 Control System

The control system or autopilot is a very important part of a missile system. The thrusting missile is unstable in flight and would soon tumble hopelessly without a properly designed autopilot. The presence of structural bending vibrations makes this stability problem much more complicated. We can easily demonstrate this for ourselves by first taking a relatively rigid yardstick in the hand and balancing it upright by applying only vertical and lateral forces at its base. The yardstick is balanced with ease. If this yardstick is now replaced by a long flexible reed or wire, the task of balancing becomes very difficult.

The essential function of the autopilot is to sense the missile attitude and angular velocity and provide engine angular deflections, and hence a lateral component of the thrust, in accordance with these sensed

quantities so as to maintain the missile at a desired attitude. The problems of control system design are treated extensively elsewhere, so that in this report the autopilot will appear to a large extent as an unobtrusive black box. In order to provide the reader with something more concrete, however, a simplified hydraulic servo will be presented in block diagram form.

2.4 Propulsion System

The propulsion system characteristics will enter the equations of this section only in a fairly superficial way. The propulsion system is taken to consist of nozzles having mass and moment of inertia which rotate about gimbal points and thereby change the direction of a steady thrust vector.

3. SIMPLIFIED EQUATIONS OF MOTION

The equations of motion that follow (as in reference 5) assume that all slowly varying quantities such as missile mass, axial acceleration, liquid levels, mode shapes and frequencies, etc., can be treated as fixed. It must therefore be emphasized that the resulting equations are valid only for a few seconds at any selected point along the trajectory; however, this is sufficient to study "high" frequency in-flight dynamics.

3.1 Missile Deflections

In order to describe the motion of the missile in-flight, it is necessary to know the motion of each section of the missile as a function of time. Once the engine start transient has damped out (this problem is considered in the next section), variations in axial forces at frequencies high enough to excite longitudinal vibrations (with the exception of engine noise, which is an entirely different type of problem) are very small so that all longitudinal deflections are neglected here. The position of each section of the missile can be described by two functions, $u(x, t)$, the lateral deflection of each point along the missile; and $\psi(x, t)$, the angle through which each section rotates relative to the moving axes. See Figure 6.

These functions can be written as

$$u(x, t) = C_0(t) + xC_1(t) + \sum_{n=1}^{\infty} \phi_n(x) q_n(t) \quad (9)$$

$$\psi(x, t) = C_1(t) + \sum_{n=1}^{\infty} \psi_n(x) q_n(t) \quad (10)$$

where x is measured from the missile center of gravity.

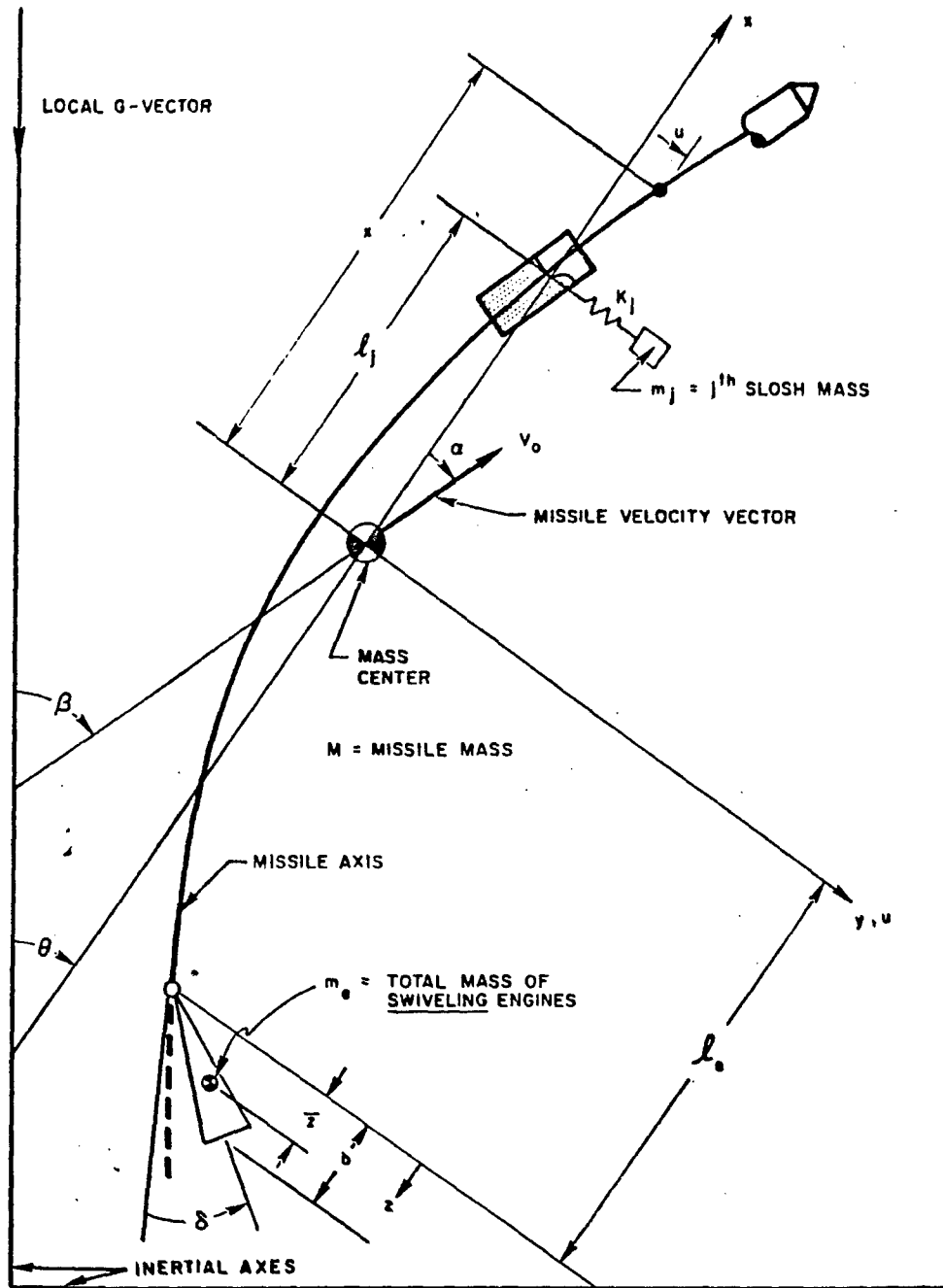


Figure 6. Geometry and Coordinate System

The functions $\phi_n(x)$ and $\psi_n(x)$ are the sloshing-bending modes described earlier, and $q_n(t)$ are the generalized coordinates of these modes and represent the amplitude that must be assigned to each mode at any instant. The time functions $C_0(t)$ and $C_1(t)$ represent a rigid-body translation and rotation, respectively, of the missile.

These quantities can be defined so that the total angular and lateral momentum with respect to the moving axes is independent of the engine deflection δ . To do this, C_0 and C_1 are adjusted so that any momentum created by engine motion is cancelled by rigid-body motions of the missile as a whole. Applying this condition, C_0 and C_1 are given by

$$C_0 = - \frac{m_e \bar{z}}{M} \delta \triangleq -K_0 \delta$$

$$C_1 = \frac{1}{I_c} (I_e + m_e l_e \bar{z}) \delta \triangleq K_1 \delta \quad (11)$$

Where I_c is the mass moment of inertia of the entire missile (including engines) about the missile center-of-gravity, I_e is the mass moment of inertia of the swiveling engines about their gimbal points, and the other parameters are shown in Figure 6.

With these definitions of C_0 and C_1 , the total angular momentum depends only on q_n and θ . The contribution of q_n is found by first writing the equation of moment equilibrium between the inertia forces and moments and the moment due to the engine force for the missile deflected into an extreme position in the nth mode:

$$\int_l (x\rho A\phi_n + \rho I\psi_n) dx + \sum_{j=1}^N x_j m_j (\phi_{jn} + \zeta_{jn}) - (T_s + T_c) \frac{\phi_n(-l_e)}{\omega_n^2} = 0 \quad (12)$$

where T_s and T_c are engine thrusts, described in more detail later. After multiplying through this equation by \dot{q}_n , inspection of the first two terms shows them to be the moment of momentum about the missile center of gravity due to a coordinate velocity \dot{q}_n . This equation can then be used to determine the following simple expression for this momentum in the positive θ direction:

$$H_n = (T_s + T_c) \frac{\phi_n(-l_e)}{\omega_n^2} \dot{q}_n \triangleq K_{2n} \dot{q}_n \quad (13)$$

The contribution to the angular momentum due to θ is merely

$$\frac{d}{dt} (I_c \dot{\theta})$$

3.2 Rigid-Body Equations

The external forces that must be considered in writing the rigid-body equations are shown in Figure 7.

Since there may be more than one engine, and not all the engines may swivel in each plane, the total thrust is broken into two components; T_c is the total thrust of the swiveling engines, and T_s is the total thrust of the engines stationary with respect to the tangent to the missile axis at the attach point.

The equation governing rotation (pitching) about the missile center of gravity is obtained by taking moments about the center of gravity with the result (see reference 12)

$$\sum_{n=1}^{\infty} K_{2n} \ddot{q}_n + I_c \ddot{\theta} = -a_T \int_l x w(x) dx + [T_c(\delta - u_e') - T_s u_e'] l_e - (T_c + T_s) u_e \quad (14)$$

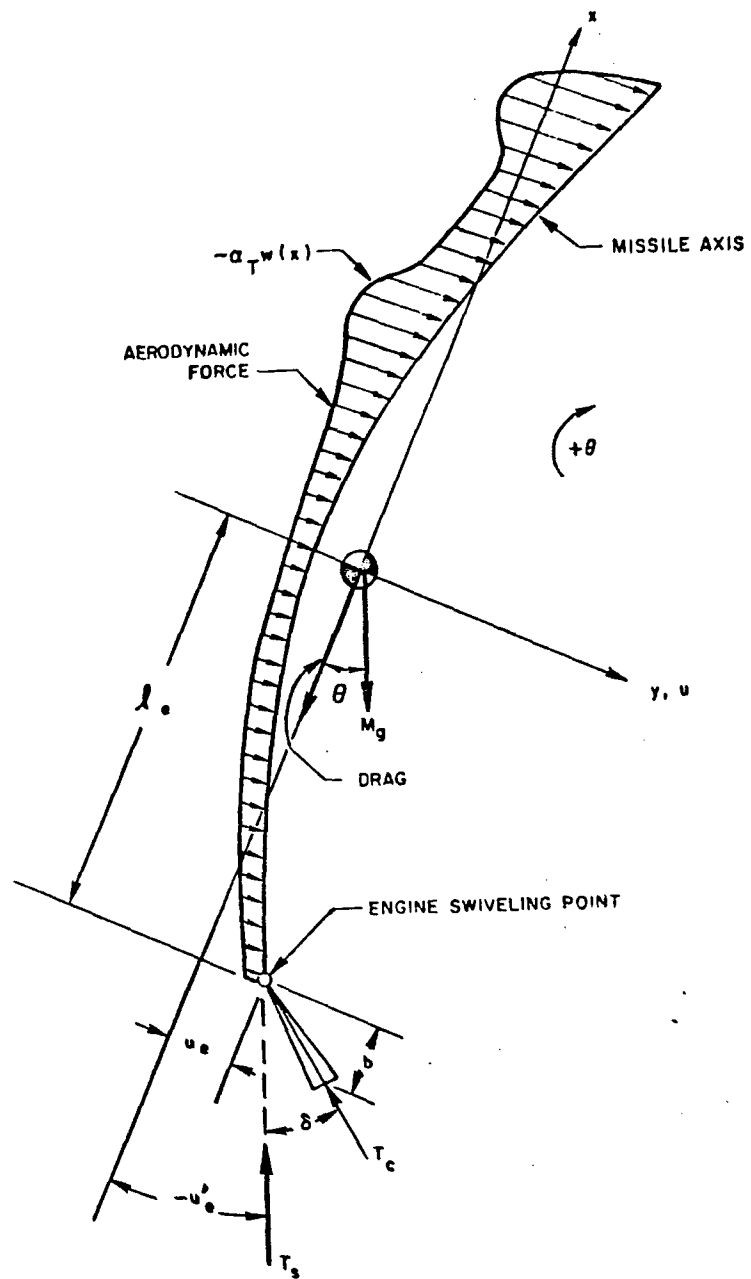


Figure 7. Forces Acting on Missile

Here

$$\alpha_T = \beta - \theta + \sum_{n=1}^N \alpha_n q_n + \frac{V_w}{V_o} + K_1 \delta - K_o \frac{\dot{\delta}}{V_o} \quad (15)$$

is the total angle of attack producing aerodynamic forces. The velocity V_w is the component of atmospheric wind velocity perpendicular to the x-axis. The angle of attack due to the sloshing is represented by $\alpha_n q_n(t)$ where α_n is the angle through which the missile airframe rotates per unit of nth "slosh mode" (a bending-sloshing mode which consists mainly of sloshing) amplitude. The summation in Equation (14) is taken only over N such "slosh modes." It is implicitly assumed in Equation (14) that the aerodynamic force depends linearly on the angle of attack, and that $w(x)$ is the running load per unit angle of attack. The dependence of the aerodynamic forces on higher powers of α , and on other quantities, such as the angular velocity of the missile, are neglected here for simplicity. These additional forces are usually small, and for many studies it is legitimate to neglect them.

The angle u_e' (the prime indicates differentiation with respect to x) is the slope of the missile axis at the engine gimbal point. It is obtained by differentiating Equation (9) and evaluating at $x = -l_e$:

$$u_e'(t) = K_1 \delta + \sum_{n=1}^{\infty} \phi_n'(-l_e) q_n \quad (16)$$

The equation governing rigid-body translation is readily obtained by summing forces in the y direction (Figure 7) with the result

$$M\ddot{y} = -a_T \int_l w(x) dx + Mg\theta + (T_c + T_s) u_e' - T_c \delta \quad (17)$$

where M is the total mass of the missile and g is the acceleration caused by gravity.

3.3 Missile Bending Equations

The bending equations (including sloshing) are most easily derived by first giving each mode a virtual displacement Δq_n and observing the work done by the forces acting on the missile. If this work is divided by the virtual displacement Δq_n , we obtain the generalized force Q_n to be used in

$$\ddot{q}_n + 2b_n \omega_n \dot{q}_n + \omega_n^2 q_n = \frac{Q_n}{M_n} + \frac{\bar{Q}_n}{M_n} \quad (18)$$

where M_n is the nth generalized mass defined by Equation 7 and \bar{Q}_n is defined in Equation 8. The generalized force, Q_n , is

$$Q_n = -a_T \int_l w(x) \phi_n(x) dx - [T_c (\delta - u_e') - T_s u_e'] \phi_n(-l_e) \quad (19)$$

In Equation (18), ω_n is the circular frequency of the nth mode and b_n is the damping ratio. Damping ratio b_n is either determined experimentally by shaking an assembled missile, or assumed conservatively small (0.5 to 1 percent of critical). It should be mentioned that the damping of a structure can seldom be represented in this way. In order that this representation be strictly correct, all damping forces would have to be of the viscous type (that is, proportional to velocity) and would have to be distributed along the length of the missile in the same way in which the mass and rotatory inertia are distributed, or in the same way in which an appropriate combination of the elastic forces are distributed. If the damping forces are distributed in any other way, application of Lagrange's equations would result in the equations of motion for the

bending modes having velocity coupling through the viscous damping forces. That is, each equation corresponding to Equation (18) would have additional terms of the form $C_m \dot{q}_m$, where $m = 1, 2, \dots$. For reasonably small values of damping, however, (corresponding to a few percent of critical damping in any mode), these coupling terms have a negligibly small effect on the motion (reference 15) and can be omitted as was done in Equation (18). Similarly, if the damping is of the hysteresis type rather than viscous, it can still be represented by an equivalent viscous damping ratio b_n for sufficiently small damping.

3.4 Control System and Engine-Swiveling Equations

The control system will be assumed to sense two quantities from gyros mounted on the missile airframe. These quantities are the attitude of the missile at the gyro station, given by $\theta_{FB} = \theta + u'_g$, and the angular velocity at that station, given by $\dot{\theta}_{FB}$, where

$$u'_g = K_1 \delta + \sum_{n=1}^{\infty} \phi'_n(t_g) q_n(t) \quad (20)$$

If the missile begins to go off course by building up an attitude θ , or if the gyros think the missile is going off course because the missile bends, giving rise to a u'_g , the control system calls for a corrective engine angle, that is, a lateral thrust component. The engine command angle δ_c is formed as a linear combination of the difference between a desired attitude θ_c and the sensed attitude θ_{FB} and the sensed rate $\dot{\theta}_{FB}$. This is expressed by

$$\delta_c = K_\theta (\theta_c - \theta_{FB}) - K_R \dot{\theta}_{FB} \quad (21)$$

where K_θ and K_R are gain constants. This engine command signal is modified by compensation networks which shape the phase and amplitude of the signal to give satisfactory stability. The resulting signal δ_c is used to open an hydraulic valve, as shown in Figure 8.

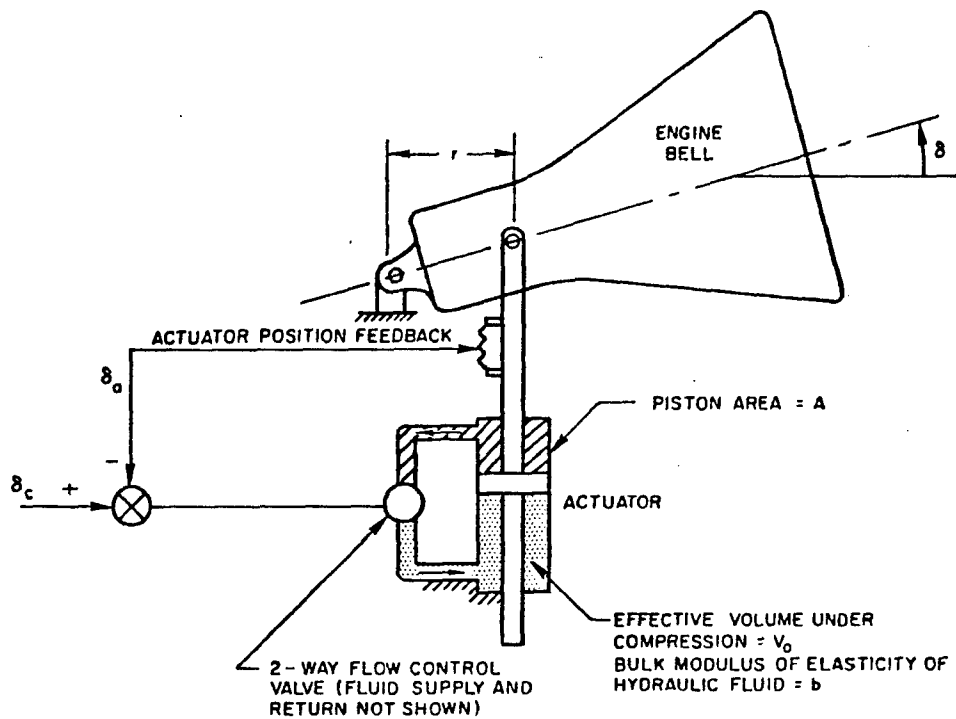


Figure 8. Schematic of Autopilot Actuator

The fluid controlled by this valve flows into an hydraulic actuator which is connected directly to the engine bell. The position of the actuator rod δ_a is sensed and subtracted from the compensated engine command angle δ_c so that it is actually the error signal $\delta_c - \delta_a$ which determines the rate of flow in the valve. If the engine angle, as measured by the position of the actuator rod, is the same as the command angle δ_c , no further fluid flows and the actuator does not move.

Going one step farther, if the compressibility of the hydraulic fluid is taken into account, there is an apparent compressibility flow which must be subtracted from the flow initiated by the error signal $\delta_c - \delta_a$. This entire process is represented conveniently in block diagram form in Figure 9. The variable s , used in this diagram, is the usual Laplace operator.

From Figure 9 it is clear that the control flow in the valve is proportional to K_v except for a small delay or valve action time τ . From this flow rate the compressibility flow Q_c is subtracted and the resultant flow is divided by Ar (defined by Figure 8) and integrated (multiplied by $1/s$) to give the actuator position δ_a , as shown. The difference between the engine position δ and the actuator position δ_a is multiplied by the equivalent torsional spring constant K_a of the actuator to give the torque acting on the engine bell. Following around the hydraulic loop, this torque divided by Ar gives the pressure in the hydraulic cylinder. This pressure, multiplied by the effective volume V_o under compression and divided by the bulk modulus of elasticity b of the fluid, gives the change in volume of the fluid caused by the pressure. The rate of change (multiply by s) of volume is the compressibility flow Q_c . The torque acting on the engine bell causes it to move according to

$$I_e \ddot{\delta} + B_e \dot{\delta} + K_e \delta = K_a (\delta_a - \delta), \quad (22)$$

where K_e is the torsional spring constant between the engine bell and the missile airframe (caused by bellows, pendulum action resulting from axial acceleration, etc.) and B_e represents any viscous damping present. Equation (22) is given in block diagram form in Figure 9. This equation is the only equation in this development of the integrated dynamic equations which is basically incomplete. Many terms have been omitted from the other equations, but they were omitted because they were small. In the case of Equation (22), however, all the interactions between engine swiveling, bending, and rigid-body dynamics

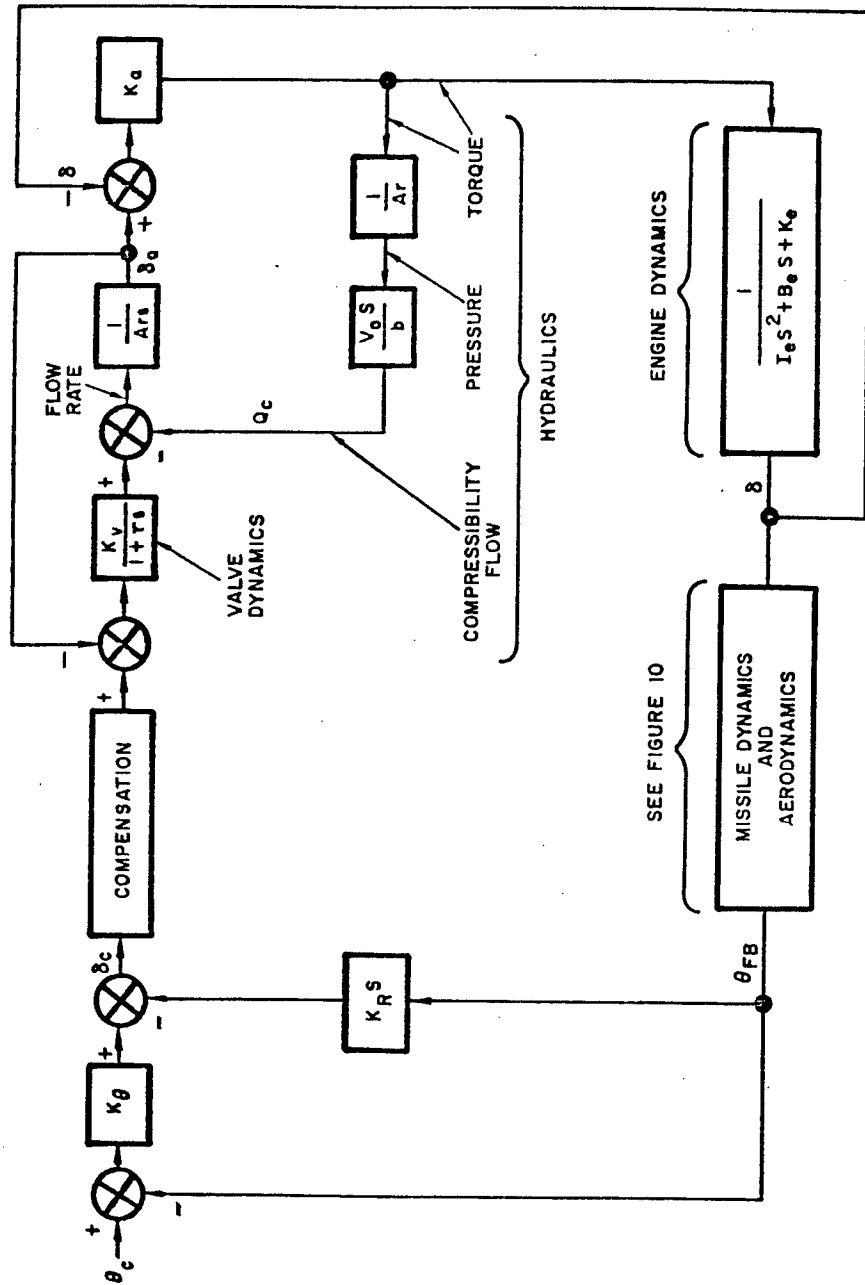


Figure 9. Block Diagram of Autopilot and Engine Dynamics

have been neglected for the sake of expediency. These interactions are important in relation to other effects included in the analysis, but most of them arise in a manner so subtle that Lagrange's equations must be resorted to to demonstrate their existence. Such a procedure is lengthy but straightforward, and the enterprising reader can derive the more complete engine-swiveling equation given by (see reference 12)

$$\begin{aligned}
 & \left[I_e - K_o m_e \bar{z} - K_1 (I_e + m_e l_e \bar{z}) \right] \ddot{\delta} + m_e \bar{z} a_x (\delta - u_e') \\
 & + (I_e + m_e l_e \bar{z}) \ddot{\theta} + m_e \bar{z} a_y + \sum_{n=1}^{\infty} \dot{q}_n \int_0^b (\rho A \phi_n z - \rho I \psi_n) dz \\
 & = K_a (\delta_a - \delta) - B_e \dot{\delta} - K_\delta \delta
 \end{aligned} \tag{23}$$

where b is the distance from the engine gimbal to the nozzle exit plane, a_x and a_y are the rigid-body accelerations in the x and y directions, and K_δ is the spring constant between the engine bell caused by a direct spring action, such as from a bellows. In spite of its being incomplete, the use of Equation (22) in conjunction with the other equations developed here would generally give adequate engineering information concerning in-flight dynamics.

3.5 Block Diagrams

Following the procedure used for the control equations, we can convert the bending and rigid-body equations into Laplace notation and draw a block diagram which represents these equations completely. Such a diagram is given in Figure 10. Only one block representing a typical bending-sloshing mode is shown in this diagram; however, it is understood that there are as many such blocks as there are modes being used. In most cases inclusion of the "slosh modes" (one for each tank) and two or three bending modes is sufficient. The summation

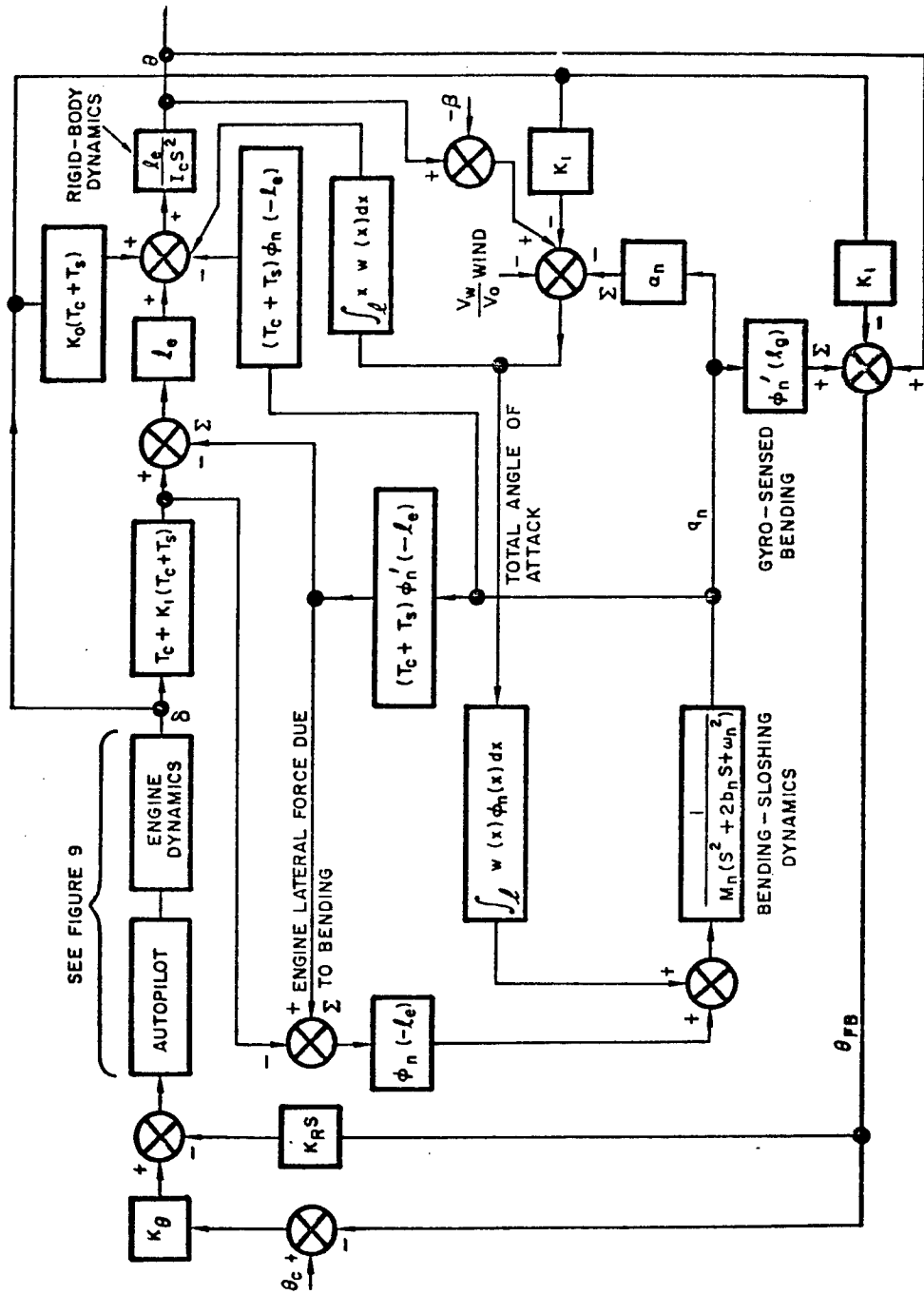


Figure 10. Block Diagram Showing Detailed In-Flight Interactions

signs given on the paths leading out of the bending-sloshing block indicate that a summation is to be made over the modes of the quantities in question.

A study of Figure 10 is enlightening in that the flow of cause and effect of each subsystem on the other can be seen without having to interpret several equations simultaneously. In addition, several significant quantities such as the engine lateral force caused by bending and the total angle of attack α_T [see Equation (15)] and their effect on the system become apparent. The complexity of Figure 10 detracts somewhat from its usefulness if we do not care to follow all the details; therefore, a functional diagram showing only the directions of the interactions is given in Figure 11.

3.6 Use of Equations

The in-flight dynamics equations developed herein have many uses. From the standpoint of the control system engineer, their most important use is to allow him to study the stability of the missile in-flight and to indicate the form of autopilot compensation required to obtain stability. The structural dynamicist sees them as a tool to determine the dynamic loads on critical sections of the missile. These loads arise from autopilot limit cycles, discrete and random gusts, staging transients, and other rapid maneuvers where the action time is of the order of the period of one of the bending modes.

For the control engineer these equations are complete as they are (with the exception of the simplifications), but the structural dynamicist must modify them slightly to insure satisfactory convergence of modal solutions, that is, a series expansion in terms of normal modes. This happens because the control engineer is interested only in displacements, whereas the structural dynamicist is interested in bending moments and shear forces as well. The convergence of series expansions of bending moments and shear forces is very poor for a beam

FUNCTIONAL BLOCK DIAGRAM

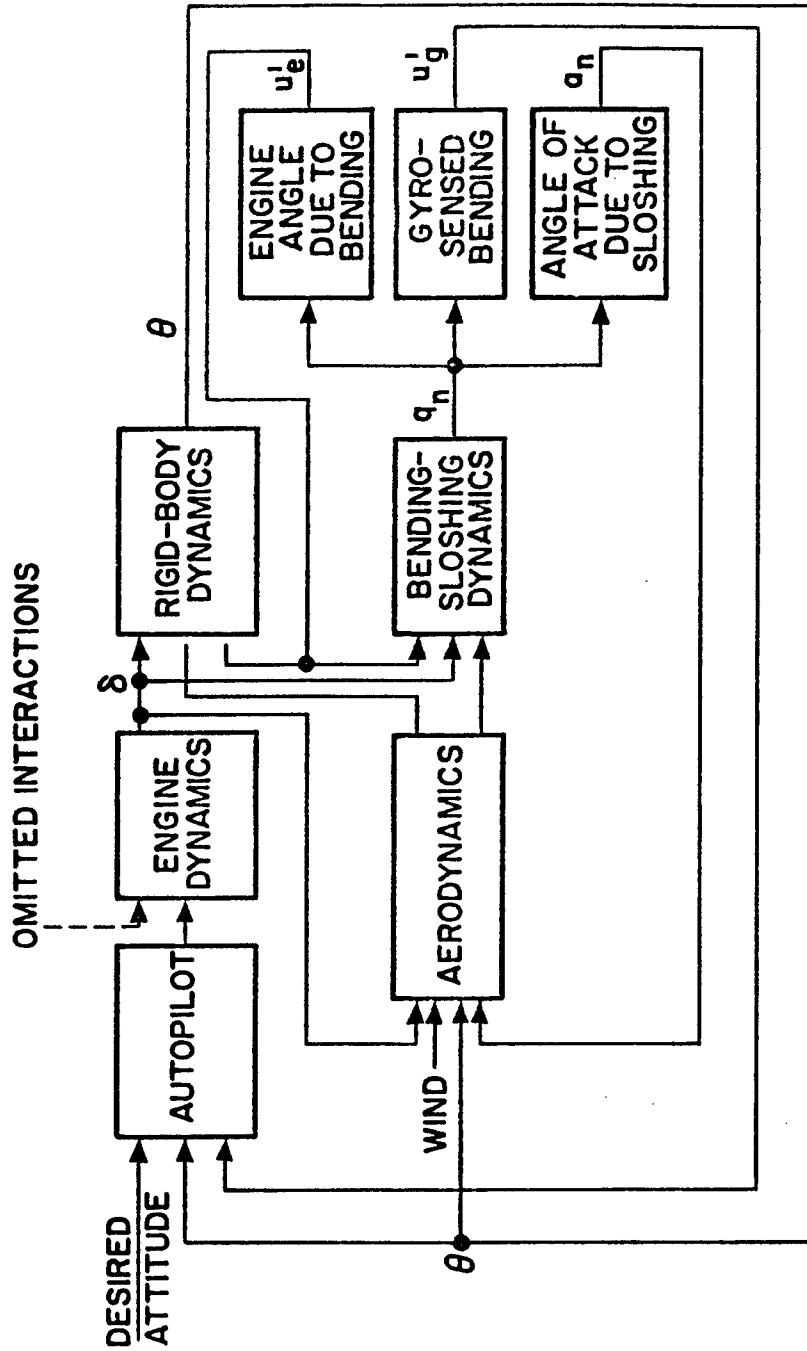


Figure 11. Functional Block Diagram

with a concentrated load (the engine force), and even in the absence of any dynamic effects at all, many modes would be needed to obtain satisfactory accuracy. On the other hand, series expansions of displacement and slope converge quite rapidly.

The difficulties associated with computing bending moments and shear force can be minimized by employing the so-called "mode acceleration" technique (reference 16). The essential feature of this method is that it separates the pseudostatic loads (loads found by rigid-body techniques) from the loads arising from the dynamic response of the missile. Thus, the poor convergence caused by discontinuities in the loading, such as a concentrated force, are taken into the pseudostatic load, and the additional load caused by dynamic bending usually converges much faster. For example, the bending moment at any station, along a missile, can be written as

$$M(x, t) = M_s(x, t) - \sum_{n=1}^{\infty} m_n(x) \frac{\ddot{q}_n(t)}{\omega_n^2} \quad (24)$$

where $M_s(x, t)$ is the pseudostatic load neglecting dynamic bending, and $m_n(x)$ is the n th eigenfunction representing the bending moment at any station. The same moment expressed without the use of the mode acceleration procedure is given by

$$M(x, t) = \sum_{n=1}^{\infty} m_n(x) q_n(t) \quad (25)$$

which converges more slowly because of the absence of ω_n^2 in the denominator. Equation (24) assumes small damping and can easily be derived from Equation (25) by using

$$\ddot{q}_n + \omega_n^2 q_n = \frac{Q_n}{M_n} \quad (26)$$

Solving for q_n from Equation (26) and substituting into Equation (25), we obtain

$$M(x, t) = \sum_{n=1}^{\infty} \frac{m_n(x) Q_n(t)}{\omega_n^2 M_n} - \sum_{n=1}^{\infty} m_n(x) \frac{\dot{q}_n(t)}{\omega_n^2} \quad (27)$$

But

$$\sum_{n=1}^{\infty} \frac{m_n(x) Q_n(t)}{M_n \omega_n^2}$$

is simply the moment that results if the system of forces, including rigid-body inertia forces, giving rise to $Q_n(t)$ is applied "statically" since it comes from the solution of Equation (26) for $\ddot{q}_n = 0$. Thus Equation (27) is identical with Equation (24). A term

$$\sum_{n=1}^{\infty} m_n(x) \frac{2b_n \dot{q}_n}{\omega_n}$$

would appear on the right-hand side of Equation (24) if damping were present in Equation (26), but the damping ratios b_n are usually quite small, and these terms can be neglected.

4. ILLUSTRATIVE EXAMPLES

4.1 Limit Cycle Response

The interaction between control system dynamics and airframe bending dynamics can force the control system into a nonlinear mode of operation which results in a limit cycle. In such a situation the control system causes the engines to gimbal continuously, searching for the correct trim condition, that is, the control system "hunts" for the correct engine swivel angle δ . The data in Figure 12 illustrate the effects that a control system limit cycle can have on dynamic loads. The data were taken from an actual case (time of flight corresponds to maximum dynamic pressure) in which the damping in the control system hydraulics became negative for large engine angular velocities δ . The negative damping caused a limit cycle whose frequency was near the first bending frequency of the missile. The control system had to be redesigned to eliminate the limit cycle.

$\frac{X}{L}$	$\frac{M_{LC}}{M_D}$	
0	1.00	$\frac{X}{L}$ = axial missile station measured from the missile tip. M_{LC} = total bending moment, control system limit cycle. M_D = total design bending moment, no limit cycle.
0.1	1.06	
0.2	1.12	
0.3	1.20	
0.4	1.27	
0.5	1.30	
0.6	1.32	
0.7	1.28	
0.8	1.04	
0.9	1.01	
1.0	1.00	

Figure 12. Dynamic Loads Generated by a Control System Limit Cycle

4.2 Response Due to Gust

It is recognized that missile inflight response analyses are complex. This is due to the interactions of the control system, aerodynamics, airframe bending dynamics, and the engine swiveling dynamics as illustrated in Figure 11. However, such analyses are tractable on electronic computers. Typical results for the inflight response of a ballistic missile during its flight through a triangular shaped (Δ) gust are shown in Figures 13 and 14. This analysis was performed on an analog computer. In Figures 13 and 14 the following nomenclature is adopted;

\ddot{q}_n = generalized bending acceleration in the nth mode
where $n = 1, 2, 3$.

α_D = angle of attack representing the gust, used as an input or driving function.

α_T = total angle of attack.

δ_N = nozzle vector angle.

M_R = pseudostatic bending moment at station x .

M_F = dynamic bending moment at station x .

M_T = total bending moment at station x .

A "mode acceleration" technique (as discussed previously) is used in the analysis and consequently one is interested in the generalized bending accelerations (\ddot{q}_n), recalling that,

$$M_T(x, t) = M_R(x, t) - \underbrace{\sum_{n=1}^3 m_n(x) \frac{\ddot{q}_n(t)}{\omega_n^2}}_{M_F(x, t)}$$

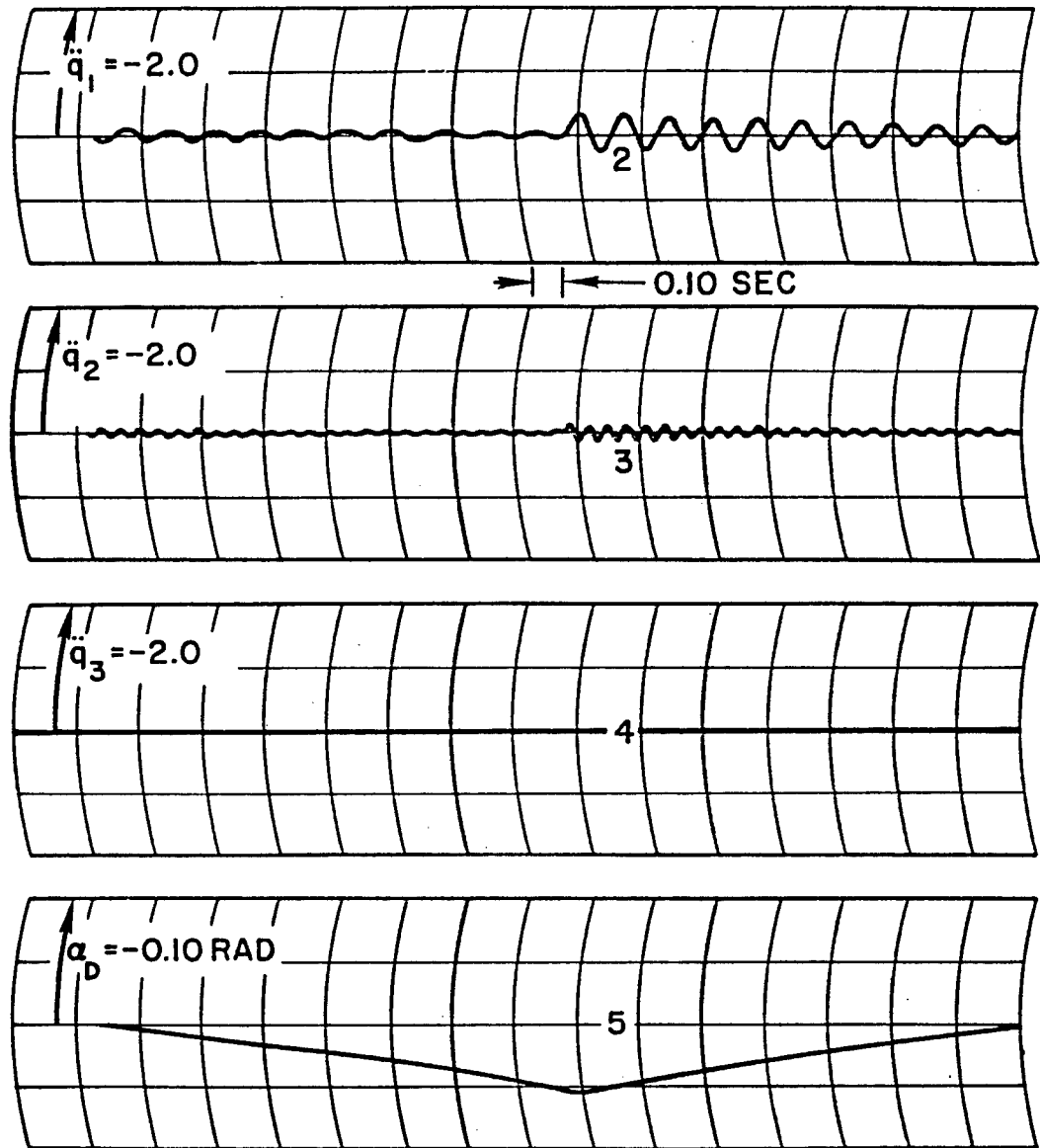


Figure 13. Bending Coordinates During Δ Gust

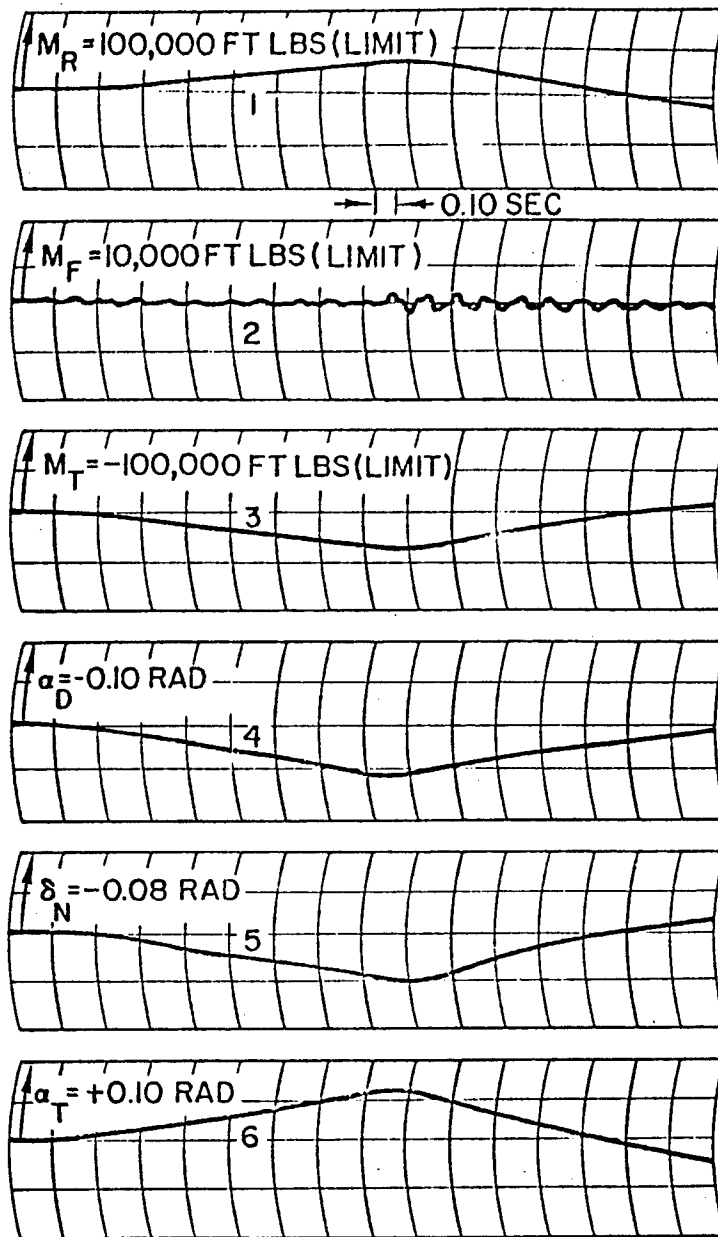


Figure 14. Inflight Response Due to Δ Gust

From Figure 13 it is clear that the major contribution to M_F comes from the first mode. In Figure 14 M_F is less than 5 percent of M_R at any time, consequently M_R is approximately equal to M_T . This result is typical for such problems if instabilities are not present even if other shapes of gust velocities are considered such as random or "1-cos" gusts.

5. PRELAUNCH-POSTLAUNCH DYNAMIC LOADS

In Section 2 the equations necessary for the computation of in-flight dynamic loads were developed. The important elements of the in-flight loads problem are the control system, the airframe bending dynamics, and the in-flight aerodynamics. In this section, three types of problems are considered. The first is concerned with the interactions between airframe bending dynamics and ground wind aerodynamic forces. The second type of problem has to do with the interactions between the axial or (longitudinal) airframe dynamics and the propulsion system. The third type of problem is concerned with the response of a constrained missile due to ground shock.

These problems fall into a general class known as prelaunch, postlaunch problems, depending on whether the dynamic loads occur before or as a result of releasing the missile.

5.1 Wind-Induced Oscillations

5.1.1 Theoretical Considerations. A missile in the prelaunch condition, that is, erected on a launch pad (Figure 15), may be exposed to ground winds which give rise to flow around the missile of large Reynolds number R^* ($R = 10^6$ based on the missile diameter). In such a flow the boundary layer on the missile is turbulent and, as a consequence, random pressure fluctuations act on the missile. These random pressure fluctuations create random lift and drag forces which in turn can induce large, oscillating displacements and bending moments in the missile.

* The Reynolds number R is defined to be $R = Ud/\nu$, where U is the undisturbed velocity of flow, d is the missile diameter, and ν is the kinematic viscosity of the flowing liquid.

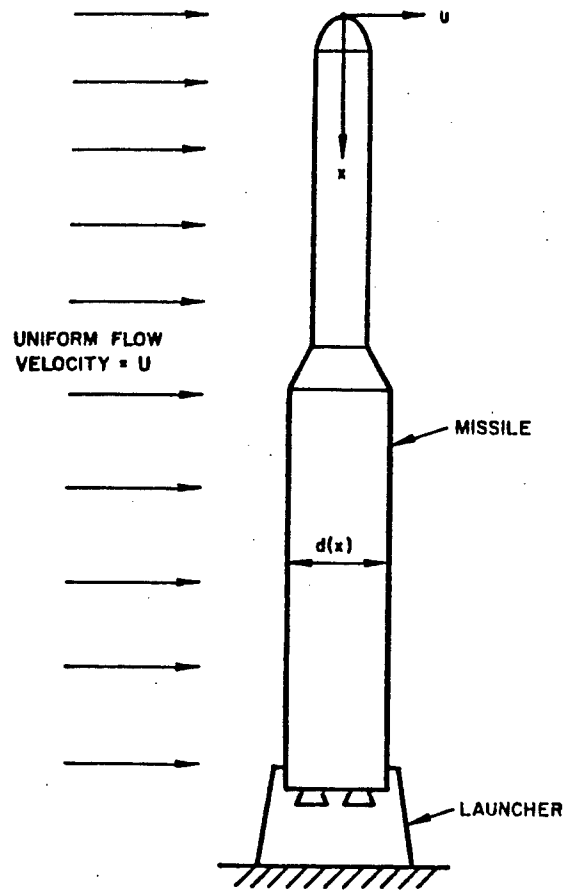


Figure 15. Missile Exposed to Ground Winds

In an air flow perpendicular to a circular cylinder, such as a missile, a great variety of changes occur with an increasing Reynolds number. Details of these changes can be found in Reference 17 and other texts in fluid mechanics. Briefly, if R is in the range of 40 to 150, the "shedding" of vortices is regular. The eddying motion in the wake is periodic both in space and time, and the flow can be approximated by the well-known Karman vortex street. The range of R between 150 and 300 is a transition range, in which the vortex shedding is no longer regular. For $R > 300$, the vortex shedding is "irregular." A predominant frequency can be determined, but the amplitude is random. Finally, at R of order 10^5 , the separation point of the boundary layer moves rearward on the cylinder and the drag coefficient decreases appreciably. The flow in the wake at these large Reynolds numbers becomes so turbulent that the vortex street pattern is no longer recognizable. Experimental results for flow around cylinders when R is larger than 10^5 are presented in Reference 18.

Consider the lateral motion of the missile in Figure 15. The applied lift force per unit length along the missile can be written as

$$L(x, t) = q(x)d(x)C_L(t) \quad (28)$$

where $q(x)$ is the dynamic pressure, $d(x)$ is the diameter, and $C_L(t)$ is the lift coefficient which varies randomly with time. Actually, C_L is a function of Reynolds number as well as of time. Therefore C_L at each missile station, depends on the diameter of the missile at that station. The dependence of C_L on R and t is such that it is not possible, in general, to express C_L as a product or sum of a function of R and a function of t . However, the experimental data of Reference 18 indicates that C_L is not a strong function of R , at least for limited ranges of R in excess of 5×10^5 . Therefore, it is reasonable to assume that a value of C_L , associated with a Reynolds number based on a representative missile diameter, should be adequate for

Equation 28. This conclusion, being founded on the data of Reference 18, is only valid for two-dimensional flow. The three-dimensional flow characteristics around the tip of a missile have a substantial effect on the total lift and drag forces. (See References 19 and 20.) However, in the absence of detailed wind tunnel input forces on particular missiles, the procedure developed herein is the best available. On the basis of limited experimental data, it can be anticipated that the results obtained will be conservative.

The lift force of Equation 28 is a random function of time since $C_L(t)$ is random in time. Problems involving random time variations are usually more conveniently treated in the frequency domain than in the time domain. The frequency representation of a random function is known as its power spectral density. Figure 16 is a typical power spectral density of lift force on a uniform cylinder. The frequency parameter, $S = \omega d / 2\pi U$, used in Figure 16 is known as the Strouhal number; the curve is normalized such that

$$\int_0^{\infty} F(S) dS = 1 \text{ or } \int_0^{\infty} F\left(\frac{\omega d}{2\pi U}\right) d\omega = \frac{2\pi U}{d}$$

By definition, if $P(\omega)$ is the power spectral density of the lift coefficient $C_L(t)$, the mean square value of C_L is given by

$$\int_0^{\infty} P(\omega) d\omega = \overline{C_L^2} \quad (29)$$

By comparing the latter two equations, the normalizing factor $K = P(\omega)/F(S)$ is evident and

$$P_L(\omega) = \frac{\overline{dC_L^2}}{2\pi U} F(s) \quad (30)$$

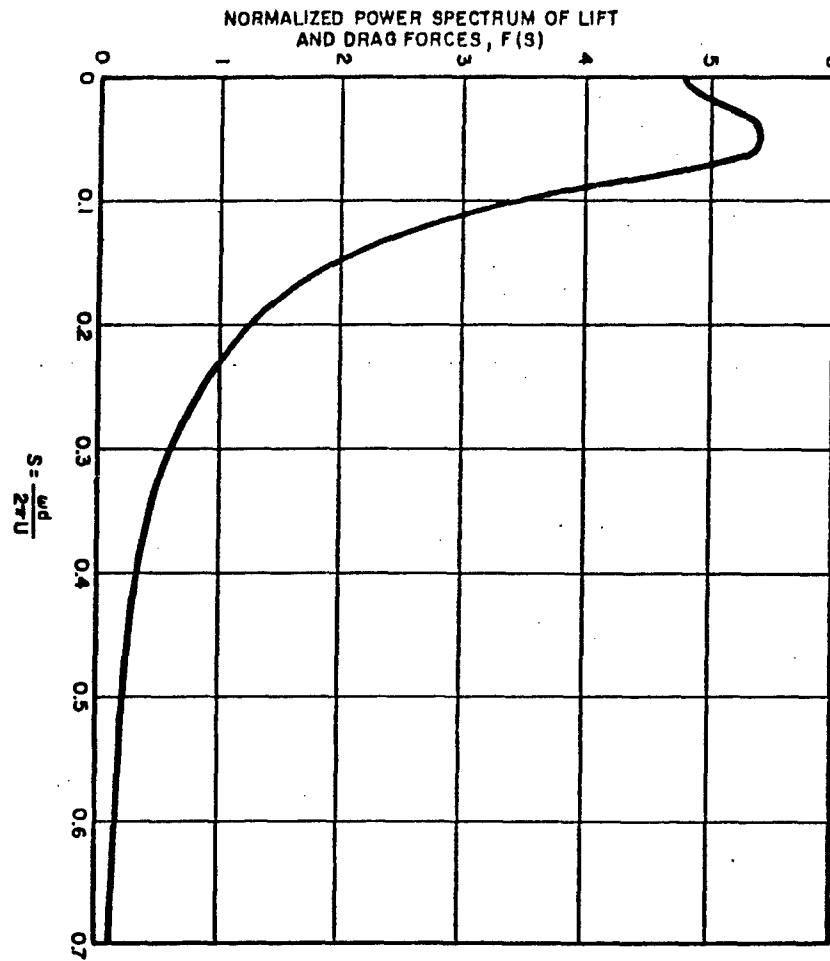


Figure 16. Normalized Power Spectrum for the Lift Force and Drag Force at Reynolds Number 1.39×10^6

Similarly, the power spectral density of the drag force is given by

$$P_D(\omega) = \frac{\overline{dC_D^2}}{2\pi U} F(S) \quad (31)$$

where $\overline{C_D^2}$ is the mean square value of the drag coefficient. The expressions for the motions of a missile resulting from random lift and drag forces are developed as follows. The displacement response of the missile, which is assumed to be a linear structure, can be expressed in terms of its principal modes as

$$u(x, t) = \sum_{n=1}^{\infty} \phi_n(x) q_n(t) \quad (32)$$

The generalized coordinates $q_n(t)$ are determined from

$$\ddot{q}_n + 2b_n \omega_n \dot{q}_n + \omega_n^2 q_n = \frac{Q_n(t)}{M_n} \quad (33)$$

where the generalized force is

$$Q_n(t) = \int_l f(x, t) \phi_n(x) dx$$

and M_n is the generalized mass of the nth mode. By assuming that the forcing function can be decomposed to

$$f(x, t) = F(x) T(t) \quad ,$$

the generalized force becomes

$$\begin{aligned} Q_n(t) &= T(t) \int_l F(x) \phi_n(x) dx \\ &\equiv T(t) W_n \end{aligned} \quad (34)$$

where

$$W_n = \int_l F(x) \phi_n(x) dx \quad \text{and} \quad F(x) = q(x) d(x)$$

For such a forcing function it is possible to find an extremely simple expression for the root mean square (rms) of the time response of the missile by assuming that the damping ratios b_n are small. The function $T(t)$ is assumed to be random and expressible in terms of a power spectral density $P(\omega)$.

To obtain the response, first notice that if $T(t)$ equals $a \cos \omega t$, the steady-state solution of the equation of motion is

$$q_n = \frac{a W_n \cos(\omega t + \theta_n)}{M_n \omega_n^2 \left\{ \left[1 - \left(\frac{\omega}{\omega_n} \right)^2 \right]^2 + \left(2b_n \frac{\omega}{\omega_n} \right)^2 \right\}^{1/2}} \quad (35)$$

The corresponding displacement is

$$u(x, t) = a \sum_n \frac{W_n \phi_n(x) \cos(\omega t + \theta_n)}{M_n \omega_n^2 \left\{ \left[1 - \left(\frac{\omega}{\omega_n} \right)^2 \right]^2 + \left(2b_n \frac{\omega}{\omega_n} \right)^2 \right\}^{1/2}} \quad (36)$$

The mean square response (which will be needed as explained later) is defined to be

$$\overline{u^2(x)} = \frac{\omega}{2\pi} \int_t^{t+2\pi/\omega} u^2(x, \tau) d\tau \quad (37)$$

$$\overline{u^2(x)} = \frac{\omega a^2}{2\pi} \int_t^{t+2\pi/\omega} \sum_n \sum_m \frac{W_n W_m \phi_n \phi_m \cos(\omega\tau + \theta_n) \cos(\omega\tau + \theta_m)}{M_n M_m \omega_n^2 \omega_m^2 \{(\omega, n)\}^{1/2} \{(\omega, m)\}^{1/2}} d\tau \quad (38)$$

This equation can be integrated by term to yield

$$\overline{u^2(x)} = \frac{a^2}{2} \sum_n \sum_m \frac{W_n W_m \phi_n \phi_m \cos(\theta_n - \theta_m)}{M_n M_m \omega_n^2 \omega_m^2 (\omega, n)^{1/2} (\omega, m)^{1/2}} \quad (39)$$

Equation 39 is the mean square response to a force distribution fixed in space and varying sinusoidally with time at frequency ω . If $T(t)$ is considered as a concentrated force acting on a unit dashpot, the average power dissipated is $a^2/2$, that is

$$\overline{E} = \frac{1}{t} \int_0^t T^2(\tau) d\tau = \frac{a^2}{2}$$

Similarly, if $T(t)$ is a random force acting on a unit dashpot, a power spectral density $P(\omega)$ can be defined for this force (with certain restrictions) such that the average power dissipated by frequency components in the range $\omega, \omega + d\omega$ is $P(\omega) d\omega$. Thus, if a random force of the form given by $f(x, t)$ acts on the missile, its response can be obtained by using Equation 39 and superimposing the responses from each frequency component of the random force, that is, replace $a^2/2$ by $P(\omega)d\omega$ and integrate over all frequencies:

$$\overline{u^2(x)} = \int_0^\infty \sum_n \sum_m \frac{W_n W_m \phi_n \phi_m \cos(\theta_n - \theta_m) P(\omega)}{M_n M_m \omega_n^2 \omega_m^2 (\omega, n)^{1/2} (\omega, m)^{1/2}} d\omega \quad (40)^*$$

* The manipulations which led to Equation 40 have been essentially intuitive and without mathematical justification. However, a mathematically rigorous treatment of the same problem yields exactly Equation 40.

It is the nature of random processes that only a statistical description is meaningful. It is quite often impossible to construct the statistics needed for a complete description; however, the mean square value, which is the second statistical moment, is usually obtainable. If the statistics of a random process are gaussian, the mean square value provides a complete description. It is for these reasons that the particular manipulations leading to Equation 40 were undertaken.

In evaluating the integral in Equation 40, a simplification can be made if the damping ratios b_n are small and if $P(\omega)$ is a smooth function as compared to the resonant peaks of the structure. In such a case, the largest contributions to the integrand are those terms for which $n = m$ because near each resonance $\omega = \omega_n$ the radicals in the denominator become very small. By neglecting the terms for which $n \neq m$,

$$\overline{u^2(x)} = \int_0^{\infty} \sum_n \frac{W_n^2 \phi_n^2 P(\omega)}{M_n^2 \omega_n^4 \left\{ \left[1 - \left(\frac{\omega}{\omega_n} \right)^2 \right]^2 + \left(2b_n \frac{\omega}{\omega_n} \right)^2 \right\}} d\omega$$

or

$$\overline{u^2(x)} = \sum_n \frac{W_n^2 \phi_n^2}{M_n^2 \omega_n^4} \int_0^{\infty} \frac{P(\omega)}{\left[1 - \left(\frac{\omega}{\omega_n} \right)^2 \right]^2 + \left(2b_n \frac{\omega}{\omega_n} \right)^2} d\omega \quad (41)$$

If $P(\omega)$ is a constant, no further assumptions need be made because each term in the foregoing equation is easily integrated. Remembering that the integrand is a function with very steep peaks at each ω_n , we can make another simplifying assumption. Since the integrand has these steep peaks near $\omega = \omega_n$, the main contribution to the integral comes when $P(\omega) = P(\omega_n)$; thus a good approximation results if $P(\omega)$ is taken as $P(\omega_n) = \text{constant}$ for each term.

Then

$$\overline{u^2(x)} = \sum_n \frac{W_n^2 \phi_n^2(x)}{M_n^2 \omega_n^4} \frac{\pi \omega_n}{4b_n} P(\omega_n) \quad (42)$$

A similar expression is derived in Reference 21. Substituting for $P(\omega_n)$ from Equation 30 yields

$$\overline{u^2(x)} = \frac{dC_L^2}{8U} \sum_n \frac{W_n^2 \phi_n^2(x)}{b_n M_n^2 \omega_n^3} F(S_n) \quad (43)$$

It follows from Equation 4 that the mean square bending moment along the missile in the lift plane is

$$\overline{M^2(x)} = \frac{dC_L^2}{8U} \sum_n \frac{W_n^2 \left[EI(x) \frac{d\psi_n}{dx} \right]^2}{b_n M_n^2 \omega_n^3} F(S_n) \quad (44)$$

The mean square response in the drag plane can be obtained from this expression if C_L^2 is replaced by C_D^2 .

The other wind force acting per unit length along the missile is the steady-state drag force defined as

$$F_{DS}(x) = C_{DS} q(x) d(x) \quad (45)$$

where C_{DS} = steady-state drag coefficient

$q(x)$ = dynamic air pressure at station x

For purposes of analysis, the responses in the drag and lift planes are added vectorally. For example, the peak displacement of the missile at station x is defined as

$$u_{\max}(x) = \left[(u_{DS} + 3u_{OD})^2 + (3u_{OL})^2 \right]^{1/2} \quad (46)$$

where u_{DS} = steady-state drag displacement

u_{OD} = root mean square value of the oscillatory drag displacement

u_{OL} = root mean square of the oscillatory lift displacement

It is assumed that the oscillatory lift and drag displacements have "normal" distributions. The root mean square values of these responses are equivalent to the standard deviations (sigma) since the "means" are zero.

The use of 3σ (3 times root mean square) values in Equation 46 implies that 99.73 percent of the time the peak oscillating lift and drag displacements will be less than the 3σ value. Equation 46 also implies that the oscillatory components of the lift and drag displacement reach their maximum at the same time, which is certainly conservative.

5.1.2 An Example. An indication of the magnitude of bending moments which may be induced by a strong ground wind acting on a large ballistic missile may be obtained from Figure 17. In this case a typical intercontinental ballistic missile is assumed to be erected on a surface launcher in the vertical position and exposed to a uniform steady 60-mph wind. The steady-state drag coefficient is assumed to be 0.55, and the predominant component of oscillatory response in both the drag and lift planes is at the first bending mode frequency of the missile. The bending moments at several points along the missile are shown in Figure 17.

As can be seen from these figures, a strong ground wind can easily impose loadings on a missile which could be catastrophic if not taken into account in the structural design of the airframe or if the missile is not otherwise protected. These figures also indicate

Distance from Missile Base, in.	Bending Moments, in. lb. $\times 10^{-5}$			
	M_{DS}	$3M_{OD}$	$3M_{OL}$	M_R
0	15.07	19.54	63.50	72.32
150	9.82	14.10	44.80	51.59
350	4.84	7.33	23.80	26.75
650	0.80	0.78	2.52	2.97

Figure 17. Bending Moments in a Typical Missile Exposed to a Uniform 60-mph Wind

the fallacy of using just the steady-stage drag response as a design criteria, since the maximum oscillatory components greatly exceed the steady-state response.

5.2 Launching in a Wind

5.2.1 Solution of the Problem. In the prelaunch condition, the missile is bent over by a steady wind and is also oscillating in its various constrained modes because of the vortex shedding previously discussed. The transients that occur in the postlaunch or free-free condition depend very strongly on the deflected shape and velocity of the missile just before release. It would be desirable to find the initial condition that gives the highest postlaunch loads, but with the missile oscillating in several modes with random phase, it is impossible to say a priori what condition would give the largest loads. It seems evident, however, that for any given constrained mode the resulting free-free loads will be largest if the missile is released when it is bent over to its maximum value. Loads indicative of the most severe postlaunch loads likely to occur can be obtained if the postlaunch transients are computed using as initial conditions the missile bent into each of its constrained modes which have appreciable amplitude because of wind-induced oscillations. This means a separate computation for each prelaunch (constrained) mode and a computation for the initial static deflection caused by steady drag.

As an example of the procedure involved in computing the postlaunch transients, consider a case in which the missile is bent into a deflection curve given by $y_0(x)$ as shown in Figure 18. The function $y_0(x)$ could represent any of the displacements discussed earlier, but for this example it will be assumed to be due only to a steady wind. The procedure to be followed here is to represent the missile in the postlaunch condition in terms of its free-free modes $\phi_n(x)$, $\psi_n(x)$ with generalized coordinates $q_n(t)$. Assuming that the free-free modes (ϕ_n, ψ_n) have been obtained from Equation 6, the problem is to determine the generalized coordinates appearing in Equations 9 and 10, that is, solve Equation 18 subject to the appropriate initial conditions. For the sake of convenience, the pertinent equations are collected here:

$$u(x, t) = C_0(t) + xC_1(t) + \sum_{n=1}^{\infty} \phi_n(x)q_n(t) \quad (9)$$

$$\psi(x, t) = C_1(t) + \sum_{n=1}^{\infty} \psi_n(x)q_n(t) \quad (10)$$

$$EI \frac{\partial \psi}{\partial x} = -M \quad (4)$$

$$KAG \left(\frac{\partial u}{\partial x} - \psi \right) = V \quad (5)$$

$$\ddot{q}_n + 2b_n \omega_n \dot{q}_n + \omega_n^2 q_n = \frac{Q_n}{M_n} \quad (18)$$

The term involving P has been dropped from Equation 5. The axial load P does not affect the bending dynamics for the problem being considered. The generalized forces Q_n and \bar{Q}_n are given by Figure 18. Here

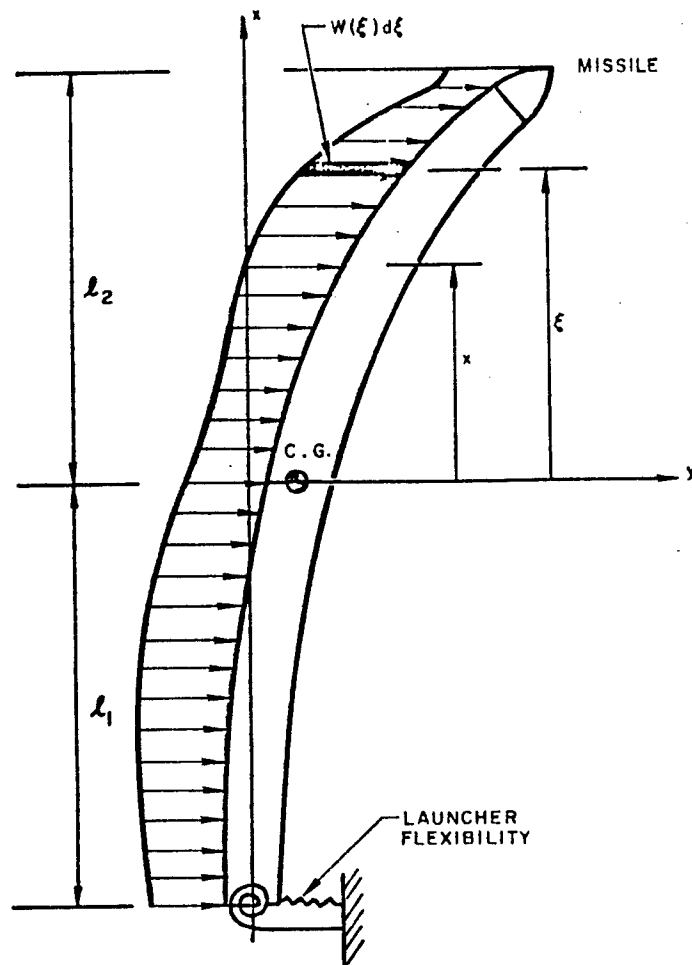


Figure 18. Coordinate System of Constrained Missile

$$Q_n = \int_l w(x)\phi_n(x)dx \text{ and } \overline{Q_n} = 0 \quad (47)$$

and are independent of time since $w(x)$ is assumed to arise from a steady wind. The solution of Equation 18 is

$$q_n(t) = \left(a_n - \frac{Q_n}{M_n \omega_n^2} \right) e^{-b_n \omega_n t} \left(\cos \omega_n t - \frac{b_n}{\omega_n} \sin \omega_n t \right) + \frac{Q_n}{M_n \omega_n^2} \quad (48)$$

where $q_n(0)$ equals a_n , $\dot{q}_n(0)$ equals zero, and b_n is assumed to be small, that is, the damped and undamped natural frequencies are essentially equal. It only remains to determine the constants a_n . To this end, the initial bending moment $M_0(x)$ and shear force $V_0(x)$ caused by the steady wind are computed from (see Figure 18)

$$-M_0 = \int_x^{l/2} w(\xi)(\xi - x) d\xi \quad (49)$$

$$V_0 = \int_x^{l/2} w(\xi) d\xi \quad (50)$$

Equations 9, 10, 4, and 5 may be combined to yield the following expansions for M_0 and V_0 :

$$-M_0(x) = EI \sum_{n=1}^{\infty} a_n \psi_n'(x) \quad (51)$$

$$V_0(x) = KAG \sum_{n=1}^{\infty} a_n (\phi_n' - \psi_n) \quad (52)$$

where prime denotes differentiation with respect to x . The constants in these expansions may now be determined with the aid of Equation 7, that is

$$\int_l EI \psi_n' \psi_m' dx + \int_l KAG (\phi_m' - \psi_m') (\phi_n' - \psi_n') dx = \begin{cases} M_n \omega_n^2 & m = n \\ 0 & m \neq n \end{cases} \quad (53)^*$$

Equation 51 is now multiplied by ψ_m' and Equation 52 is multiplied by $\phi_m' - \psi_m'$; the results are added and integrated over the length of the missile to yield

$$\int_l [M_0 \psi_m' + V_0 (\phi_m' - \psi_m')] dx = \int_l EI \psi_m' \sum_{n=1}^{\infty} a_n \psi_n' dx + \int_l KAG (\phi_m' - \psi_m') \sum_{n=1}^{\infty} a_n (\phi_n' - \psi_n') dx \quad (54)$$

A comparison of Equations 54 and 53 yields immediately

$$a_n = \frac{1}{M_n \omega_n^2} \int_l [M_0 \psi_n' + V_0 (\phi_n' - \psi_n')] dx \quad (55)$$

with the a_n 's determined, it is now possible to compute the bending moments and shear forces generated as a result of launching a missile in a wind.

5.2.2 An Example. Because the moment at the base $x = -l_1$ is the maximum moment in the constrained condition, while the moment at this station is zero for all of the free-free modes, the convergence of the initial moment expressed in terms of free-free modes is understandably poor. However, such an expansion has been made using the bending modes of an actual missile, and convergence to a reasonable engineering accuracy was obtained using six bending modes. Figure 19 shows a plot of

*The terms corresponding to the sloshing coordinates and P have been dropped from Equation 7. Experience has shown that sloshing and P are not important in the problem being considered.

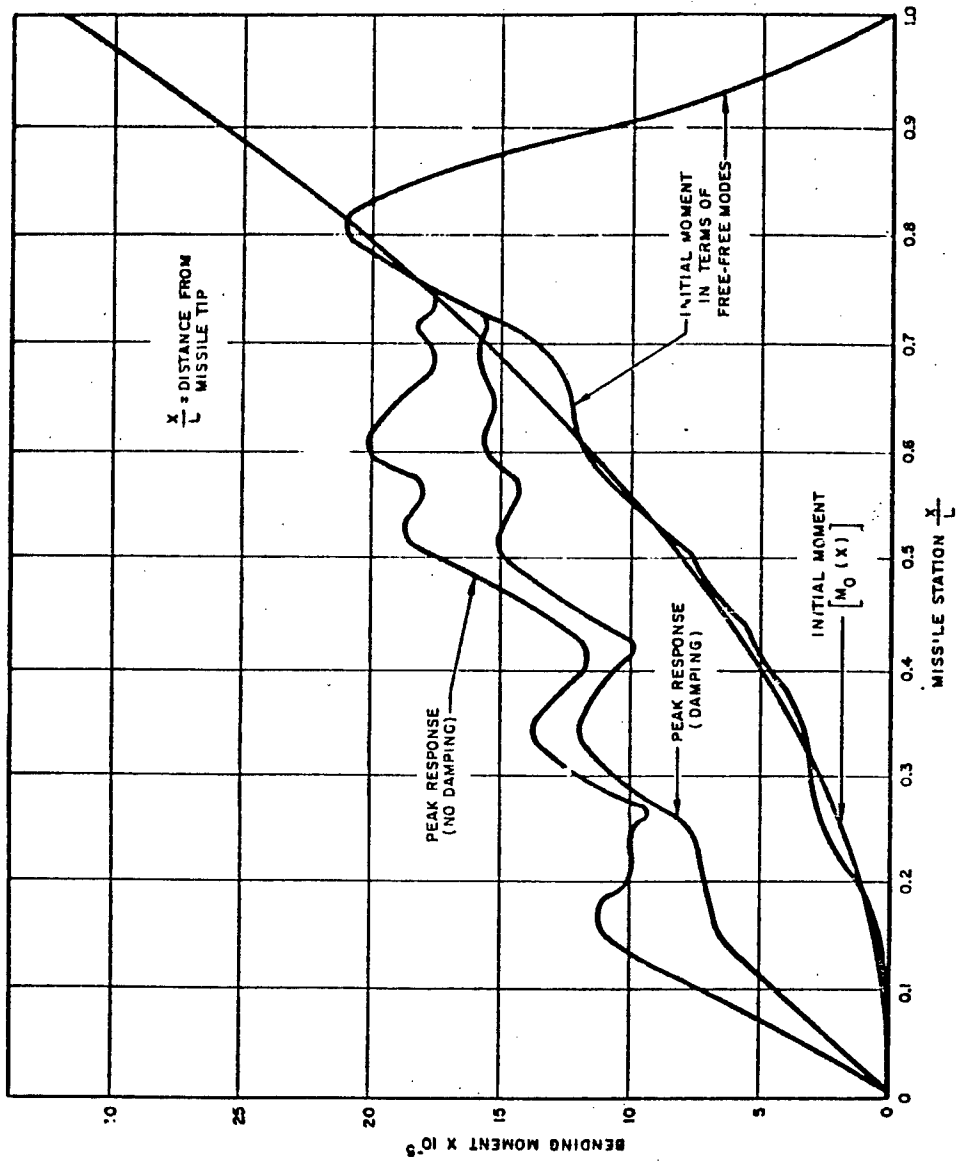


Figure 19. Absolute Maximum Bending Moments at Launch

$$\sum_{n=1}^N EI(x) a_n \frac{d\psi_n(x)}{dx}$$

for values of N from one to six. The initial moment $M_0(x)$ is also shown, and it can be seen that convergence is good for sections away from the base. Near the base, the maximum loads occur before launching so that the poor convergence here is not important. An indication of the convergence during the postlaunch transient is given by Figure 20, which shows the maximum value of $M(x, t)$ incurred during the transient at several stations of the missile.

Again, N is varied from one to six in this figure, and it can be seen that the additional moment due to the sixth mode is not too large. These computations were made with no postlaunch damping (that is, $b_n = 0$). When the damping was included, the convergence was better, particularly near the center of the missile where the lower free-free modes contribute strongly to the moment. At these stations, moments caused by the higher modes were damped out by the time the moments caused by the lower modes became in phase. A comparison of the peak postlaunch moments with and without damping is shown in Figure 19. The amount of damping used in the analysis was

$$b_n = 0.02$$

Figure 19 also indicates the importance of the postlaunch transient. Notice that in the prelaunch condition the bending moments near the tip of the missile are quite small, whereas during the postlaunch transient the bending moments become quite appreciable because of the unloading wave induced by the sudden release. The characteristic dip in the moment curve at station 0.44 of Figure 19 is caused by a sudden reduction in the flexural rigidity of the missile at this station. These postlaunch moments designed the forward section of the missile of this example. Details of this analysis can be found in Reference 22.

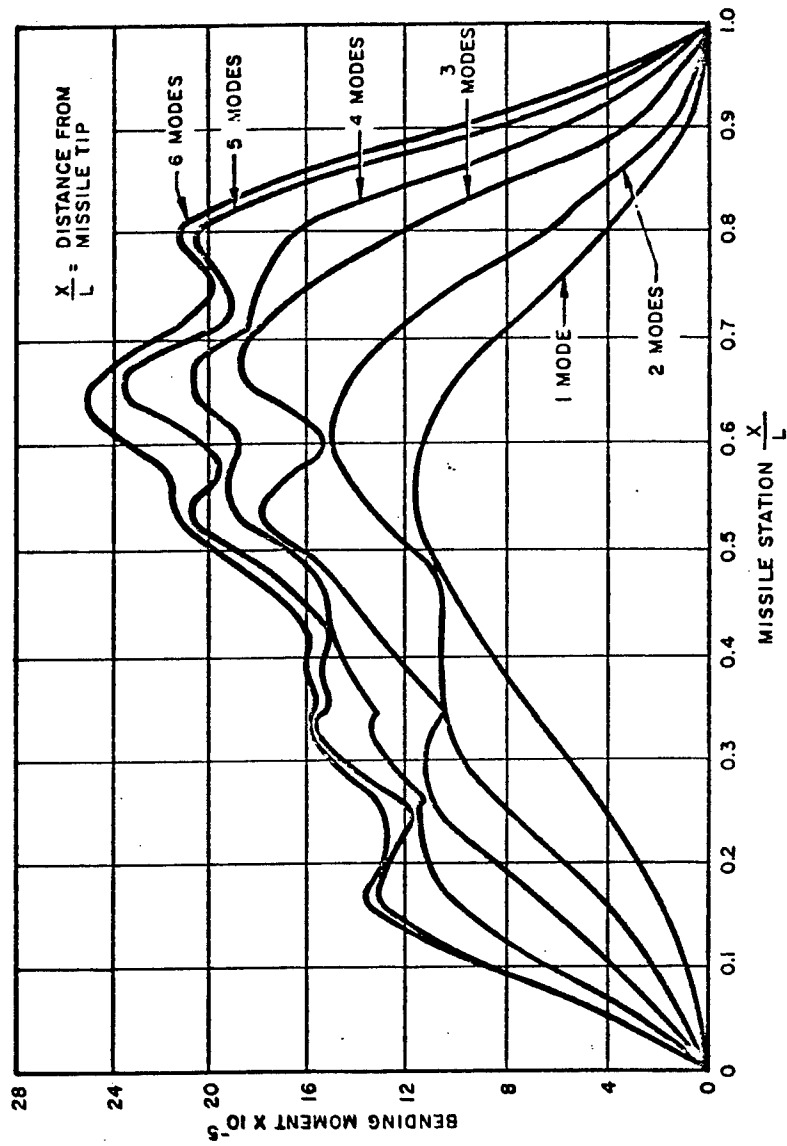


Figure 20. Absolute Sum of Peak Mode Responses of Bending Moments Due to Sudden Release from Initial Deflection

5.3 Effects of Thrust Build-up

In this section the problem of determining the dynamic loads generated by an engine start transient is considered. This problem differs from those discussed in previous sections in that the longitudinal rather than the bending dynamics of the airframe is involved.

5.3.1 Theoretical Considerations. Consider a missile erected on and attached to a launch stand (see Figure 21). At time $t = 0$ the engines are started, generating a time dependent thrust $F(t)$. The problem is to determine the response of the airframe to $F(t)$.

Experimental data have confirmed that the longitudinal dynamics of a missile airframe are adequately represented by simple, one-dimensional, beam theory. Therefore, the longitudinal response of the missile is determined from

$$a^2(x) \frac{\partial^2 u(x, t)}{\partial x^2} = \frac{\partial^2 u(x, t)}{\partial t^2} \quad (56)$$

subject to the boundary conditions. Here

$$\frac{\partial u(0, t)}{\partial x} = 0, \quad \frac{\partial u(S, t)}{\partial x} = -\frac{1}{A(x)E} [F(t) + K_0 u(S, t)] \quad (57)$$

where

$$a^2(x) = \frac{EA(x)}{m(x)}$$

E = modulus of elasticity

$A(x)$ = cross-sectional area of the load carrying portion of the airframe

$m(x)$ = mass per unit length of the airframe

$u(x, t)$ = axial displacement of the airframe

x = axial coordinate measured from the missile tip

K_0 = spring constant of the launcher

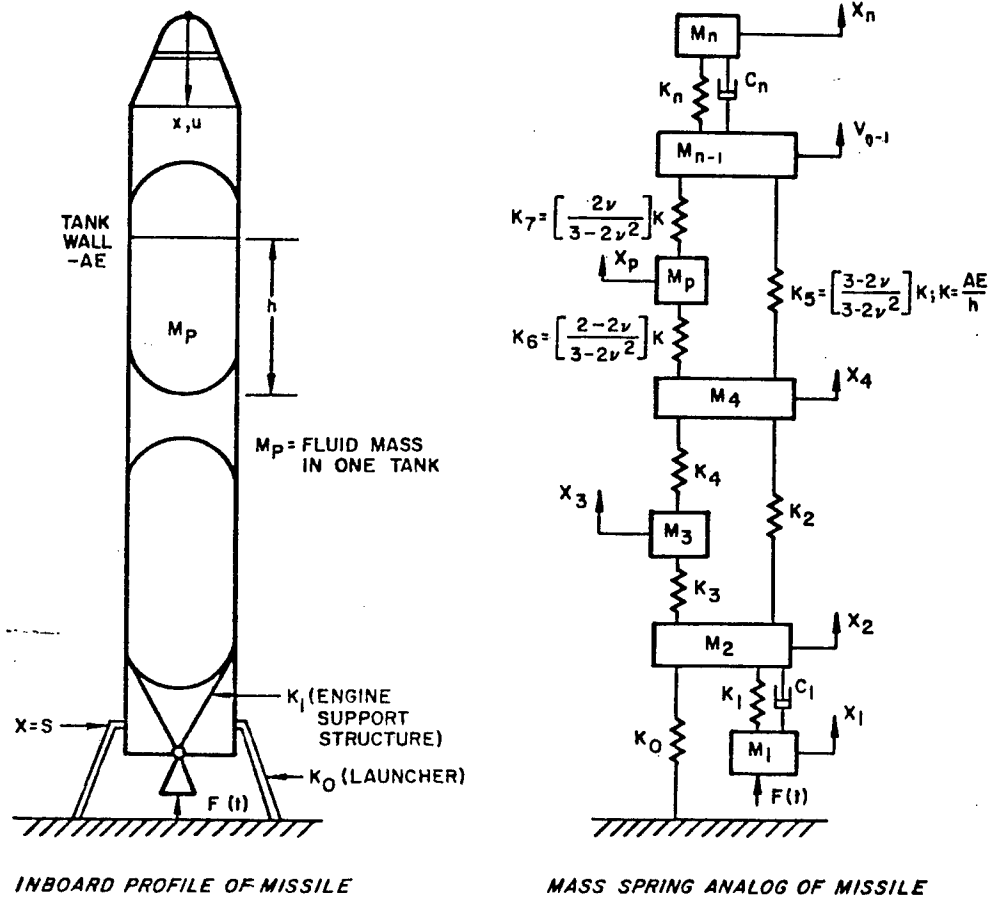


Figure 21. Inboard Profile and Mass-Spring Analog of Missile

A direct integration of Equation 56 is usually quite difficult, especially when the effects of liquid propellants are included. Therefore, rather than attempt a direct solution of Equation 56, it is far more convenient to replace the continuous airframe by a lumped spring-mass analog. A typical decomposition of an airframe into a spring-mass system is shown in Figure 21.

The general procedure used to arrive at such an analog is to divide the airframe into a number of sections, replacing the distributed mass of each section by a single mass placed at the center of gravity of each section; the masses are joined by springs whose stiffnesses are equal to the stiffness of the airframe structure between the masses. The inclusion of propellant effects requires special treatment. The hydrostatic pressure created by the effective weight of accelerating propellants causes the propellant tanks to bulge, which in turn shifts the center of gravity of the propellant mass. A computation of these events leads to expressions for effective spring constants of the form given by K_5 , K_6 , and K_7 of Figure 21. The expressions for these constants are derived in Section 1 of the Appendix.

The equations of motion of the spring-mass analog can be written by inspection. Some of these equations are

$$\begin{aligned}
 M_n \ddot{x}_n + K_n(x_n - x_{n-1}) + C_n(\dot{x}_n - \dot{x}_{n-1}) &= 0 \\
 M_{n-1} \ddot{x}_{n-1} + K_7(x_{n-1} - x_p) + K_5(x_{n-1} - x_4) + K_n(x_{n-1} - x_n) \\
 &\quad + C_n(\dot{x}_{n-1} - \dot{x}_n) = 0 \\
 M_p \ddot{x}_p + K_6(x_p - x_4) + K_7(x_p - x_{n-1}) &= 0
 \end{aligned}$$

$$\begin{aligned}
& M_4 \ddot{x}_4 + K_4(x_4 - x_3) + K_2(x_4 - x_2) + K_6(x_4 - x_p) \\
& \quad + K_5(x_4 - x_{n-1}) = 0 \\
M_2 \ddot{x}_2 + K_1(x_2 - x_1) + C_1(\dot{x}_2 - \dot{x}_1) + K_2(x_2 - x_4) + K_3(x_2 - x_3) \\
& \quad + K_0 x_2 = 0 \qquad x_2 \leq \frac{W}{K_0} \\
M_2 \ddot{x}_2 + K_1(x_2 - x_1) + C_1(\dot{x}_2 - \dot{x}_1) + K_2(x_2 - x_4) \\
& \quad + K_3(x_2 - x_3) + W = 0 \qquad x_2 > \frac{W}{K_0} \qquad (58)
\end{aligned}$$

where

$$W = \sum_{i=1}^n m_i g$$

The limits on the last two equations of 58 account for the possibility of the missile separating from the launcher. The solution of these equations provides axial loads F_n , for example,

$$F_n = K_n(x_n - x_{n-1}) + C_n(\dot{x}_n - \dot{x}_{n-1})$$

and accelerations \ddot{x}_n for different sections of the missile. Since the coordinates originate from the equilibrium position, the absolute acceleration of any mass will be $\ddot{x}_n + g$, where g is the acceleration caused by gravity. Similarly, the total axial load at station n equals $K_n(x_n - x_{n-1}) - m_n g + C_n(\dot{x}_n - \dot{x}_{n-1})$. This choice of coordinates is made in order to eliminate the necessity of computing initial displacements and setting them as initial conditions on a computer. The initial displacements for the equations here are all zero, whereas if all spring deflections were measured from their

free length, the deflection of each spring under the weight of the masses above it would have to be used to determine initial conditions. In a more complicated model with springs spanning across several masses, solution of the static problem is more tedious so that the use of coordinates measured from equilibrium is even more strongly indicated.

In many engine thrust transient response problems the effect of damping in the missile is very important. Hence, an estimate of the modal damping (possibly an experimental value) for the structure is necessary to determine the values of dashpots C_n , which are located between masses as shown in Figure 21. If the modal damping b_n in the missile is small, it can be shown (Reference 15) that a good approximation for b_n is given by

$$b_n = \sum_{j=1}^P C_j \frac{[\phi_n(x_j) - \phi_n(x_{j+1})]^2}{2\omega_n M_n} \quad (59)$$

where

b_n = percent of critical viscous damping
in nth mode

C_j = dashpot constant at station j

P = total number of dashpots

$\phi_n(x_j) - \phi_n(x_{j+1})$ = relative displacement in dashpot j,
for the nth mode

ω_n = circular frequency of nth mode

M_n = generalized missile mass for the nth
mode

$$\sum_{i=1}^N m_i \phi_n^2(x_i)$$

N = total number of masses

Equation 59 provides the necessary values of the dashpot constants to maintain the desired modal damping. A set of P simultaneous equations are formed with P dashpot constants, C_j as unknowns.

Equation 58 can be written in matrix form as follows:

$$[A]\{\ddot{x}\} + [B]\{\dot{x}\} + [C]\{x\} = 0 \quad (60)$$

where

$$\begin{aligned} [A] &= \text{mass matrix} \\ [B] &= \text{damping matrix} \\ [C] &= \text{stiffness matrix} \\ \{ \} &= \text{a column matrix} \end{aligned}$$

For purposes of computing longitudinal modes and natural frequencies, the damping is assumed to be negligible, and the time dependence of the displacements is sinusoidal with frequency ω . Equation 60 then takes the form

$$([C] - \omega^2[A])\{x\} = 0 \quad (61)$$

Equation 61 is the classical form for an eigenvalue problem in matrix notation. The solution of 61, yields the natural frequencies ω_n and mode shapes $\phi_n(x)$. With the mode shapes available, the response of the spring-mass analog can be written as

$$u(x, t) = \sum_{n=1}^N \phi_n(x) q_n(t) \quad (62)$$

with the generalized coordinates $q_n(t)$ given by

$$\ddot{q}_n(t) + 2b_n \omega_n \dot{q}_n(t) + \omega_n^2 q_n(t) = \frac{F(t)\phi_n(x_s)}{M_n} \quad (63)$$

Equations 62 and 63 are valid, independent of whether the missile is resting on or has left the launcher, the only difference being that the mode shapes ϕ_n are different in each case.

Equations 62 and 63 may not represent the most convenient form of the solution. In fact, it is often much faster to solve Equation 58 directly on an analog computer rather than attempt a modal solution.

5.3.2 An Example. Figure 22 shows the effects of damping and release time on missile axial loads caused by launch and engine thrust transients. The axial loads occur in a large ballistic missile just after launch when the release time is specified at a percent of the full engine thrust. A typical engine thrust build-up curve is shown in Figure 23 with release times of the missile which correspond to the cases of Figure 22. To compare cases B and D, the differences in the loads are caused by the transients of the engine thrust which are generated in part by the rate of build-up. In case D these transients are nearly damped out, and hence for this case the results may be obtained by simply applying a step load to the end of a free-free missile of magnitude $T - W$, where T is the 100 percent thrust value and W is the total weight of the missile. To compare cases A and B, the differences in the axial loads is mainly caused by the differences in the rigid-body accelerations. The effect of damping is clearly indicated in cases B and C. Although the axial loads of Figure 22 indicate that it is advantageous to release the missile at the lowest thrust level, the combination of axial and lateral loads may indicate the necessity for a different time of release. An over-all loads picture must be examined before a release time can be specified. The lateral loads will dominate the axial loads in certain sections of the missile and vice versa. Therefore, if the lateral loads are predominant, which is usually the case at sections near the tip of the missile, it may be necessary to launch at a time when some of the contributors to lateral loads are damped out, that is, effects of engine thrust differential, which have not been treated here.

Case	Missile Station	Maximum Compressive ^a
		Axial Load
A:	125 tip	1.0 ^b
Release at 77% of full thrust	250	4.5
$b_n = 1\%$	400	12.2
$n = 1, 2, 3, 4$	800	38.8
B:	125	2.1
Release at 100% of thrust	250	11.1
$b_n = 1\%$	400	27.5
	800	64.5
C:	125	3.8
Release at 100%	250	18.0
$b_n = 0$	400	45.0
	800	73.5
D:	125	1.9
Release after a 1-second hold	250	9.7
$b_n = 1\%$	400	24.0
	800	59.0

^a Loads are normalized to (b) and occur after release (postlaunch).

Figure 22. Effect of Damping and Release Time on Missile Axial Loads due to Launch and Engine Thrust Transients

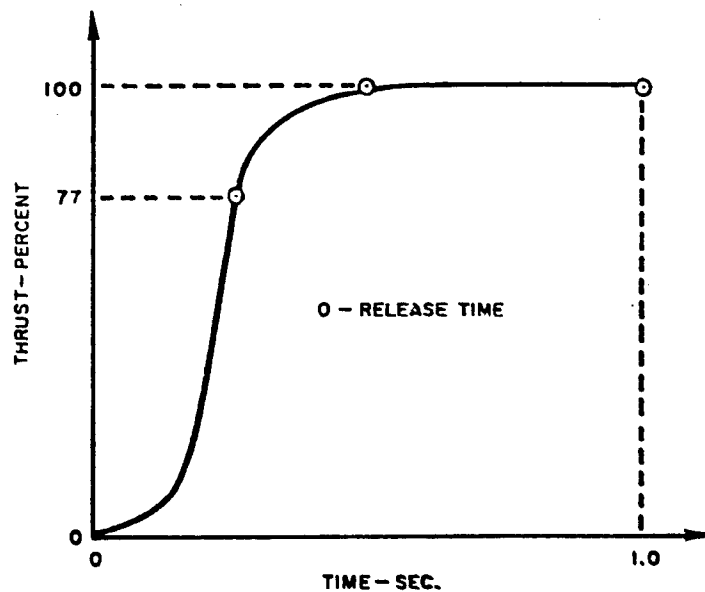


Figure 23. Engine Thrust Build-up Curve

5.4 Missile Response due to Ground Shock

Many dynamic problems are encountered before the missile is airborne, for example, in transport and ground handling, however, this section will be limited to the discussion of missile dynamic response due to ground shock.

There are many complex problems encountered in determining the responses of missiles due to ground shock and in determining the characteristics of shock isolation systems which attenuate these responses. Some investigators have examined these problems by representing a continuous structure by a single degree of freedom system. This system, however, may be inadequate or the responses such as displacements, moments and shears may be misleading. Therefore, the more difficult problems associated with a continuous structure should be investigated. A method of analysis for these problems using a "shock spectra" technique is given in Reference 25 and 26.

In this section two aspects of these problems are considered. They are:

- a) The specification of the shock environment
- b) The dynamic response of the missile to the environment.

The ground shock environment may be specified in various ways, such as by soil pressure, displacement, permanent set, velocity or acceleration. All of these may be of use in particular applications. For the purpose of this section attention is given to the displacement shock spectra (Reference 25).

Although there are certain practical difficulties, it is theoretically possible to determine the response of a structure to shock if the acceleration time input and the dynamic characteristics of the structure in terms of the principal modes frequencies, and damping are known. It is also possible to estimate upper bounds of response by means of the shock spectra and the dynamic characteristics of the structure. This latter procedure will be discussed in the determination of maximum stresses and displacements. It is pointed out to the reader that this method of determining the upper bound response of a structure due to transient excitation is also a very useful tool for problems other than ground shock. It has important applications in the specification of the type and intensities of shocks a structure must resist, and in the estimation of the strength of a structure in resistance to a variety of shocks. Such problems arise in the packaging of electronic equipments for transportation, in the resistance of a structure to earthquake, in the landing of an aircraft, in the starting shock of a rocket, and in a large variety of impact loads.

To discuss the response of missiles to ground shock, the missile is considered in a vertical position attached to a launch stand which is protected from air blast but is subjected to ground shock. (See Figure 24.) The ground shock in terms of the soil acceleration as a function of time consists of two major components: a vertical component and a component directed radially from ground zero where the blast initiates.

The dynamic characteristics of the structure are conveniently expressed in terms of the principal modes and frequencies, and structural damping. For the missile-stand combination the transverse modes are very similar to those of an elastically supported cantilever beam. The displacement of any point of the structure can then be taken as the superposition of the mode contributions.

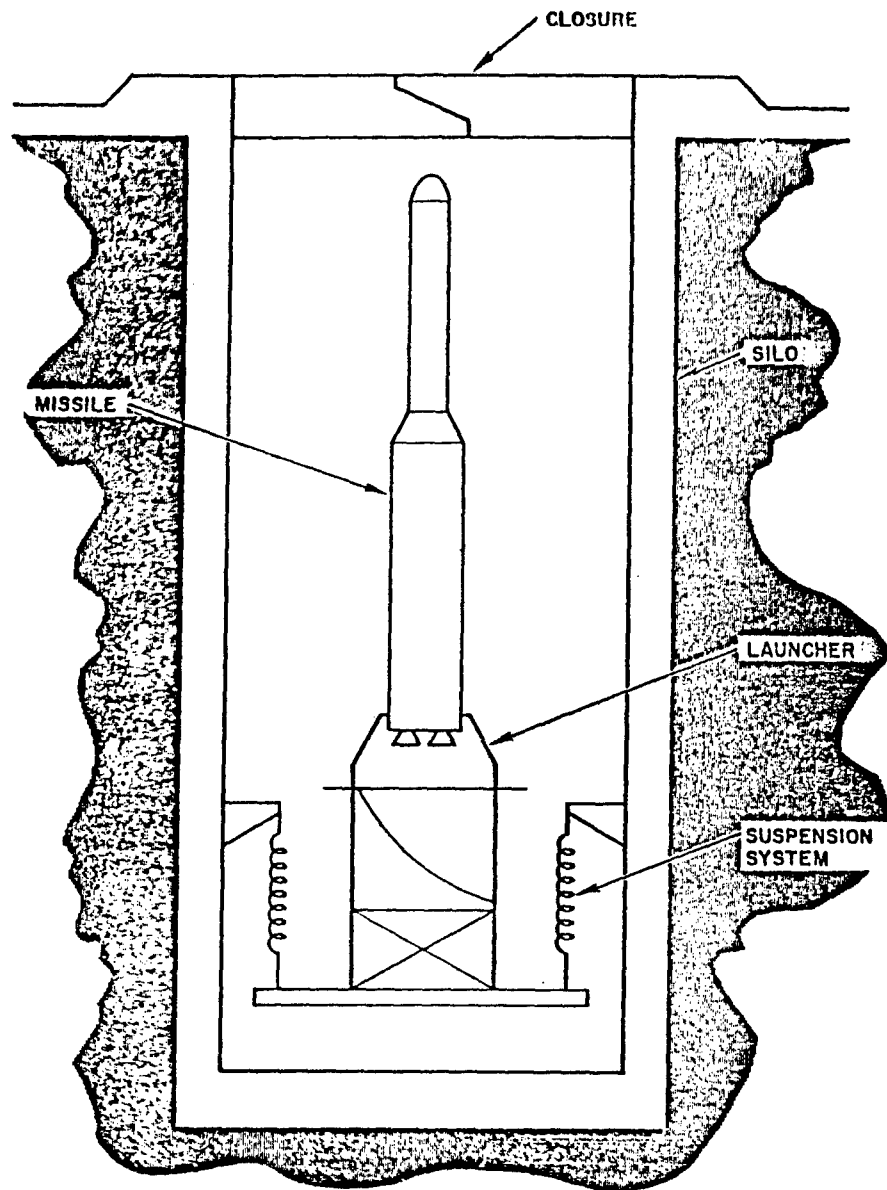


Figure 24. Missile—Launcher

The displacement of the missile relative to the ground, as shown in Figure 24 is given by,

$$u(x, t) = \sum_n \phi_n(x) q_n(t) \quad (64)$$

where

u = displacement of the structure at point x relative to the ground

q_n = generalized coordinate of the n^{th} mode

ϕ_n = value of the n^{th} mode at position x

For an acceleration input, the equation of motion for the n^{th} mode is,

$$\ddot{q}_n + 2\zeta_n \omega_n \dot{q}_n + \omega_n^2 q_n = \frac{-a(t) \int_l \rho \phi_n dx}{\int_l \rho \phi_n^2 dx} \quad (65)$$

where,

ζ_n = ratio of damping to critical viscous damping in the n^{th} mode

ω_n = circular frequency of the n^{th} mode

ρ = mass distribution per unit length

$a(t)$ = acceleration of the ground

The right hand side of this equation represents the generalized force, $a(t) \int_l \rho \phi_n dx$, divided by the generalized mass, $\int_l \rho \phi_n^2 dx$. For convenience let $\gamma_n = \int_l \rho \phi_n dx / \int_l \rho \phi_n^2 dx$. This term has been called the kinematic or distribution factor (Reference 24).

The solution to the foregoing equation of motion for small damping and for initial conditions of a , q_n , and \dot{q}_n equal to zero at $t = 0$, is,

$$q_n(t) = -\frac{\gamma_n}{\omega_n} \int_0^t a(\tau) e^{-\zeta_n \omega_n (t-\tau)} \sin \omega_n (t-\tau) d\tau$$

which when substituted into Equation 64 determines the response of the structure.

There are several practical difficulties in determining the response of the structure in the foregoing manner. Some of these difficulties come from the evaluation of the integral with practical acceleration records $a(t)$; others arise from the characteristics of the acceleration records such as statistical scatter, damping, and determination of low-frequency components. These difficulties may be present in problems other than ground shock.

It is sometimes convenient to think of the relationship of the generalized coordinates to quantities that can be measured directly without a knowledge of the ground accelerations. In effect, the structural system for which dynamic responses are to be determined is replaced by a series of single-degree-of-freedom systems. For example, the analog for the motion of each mode of the missile on the stand can be represented by a cantilever beam tuned to the principal frequency for the mode of the missile. Hence, assuming an idealized single-degree-of-freedom system such as a cantilever with an end mass, the equation of motion for the mass is,

$$\ddot{Q} + 2\zeta\omega\dot{Q} + \omega^2 Q = -a(t)$$

This equation has the same form as Equation (65), so that if the motion of the mass of the single-degree-of-freedom system is known (by measurement or other means), the generalized coordinate for the n th mode of the structure is given by

$$q_n = \gamma_n Q_n$$

and the structural response is

$$u = \sum_n \gamma_n \phi_n Q_n \quad (66)$$

Now the motion, $Q(t)$, of the mass is often difficult to measure as a complete displacement-time history. Fortunately, it is possible to make some predictions about the maximum value of the response of the structure from a knowledge of only the peak values of the response of the single-degree-of-freedom system, which are relatively easy to calculate if the pulse input is known or to measure by means of reed shock gages such as in the case of ground shock input. (See Reference 24.)

A shock gage may consist of a set of single-degree-of-freedom systems, as shown in Figure 25. The frequency spectrum of the peak displacements of the masses relative to the base which is being accelerated is called the displacement shock spectrum and is given by

$$D(\omega) = Q_{\max} = \max_{t > 0} \left| \frac{1}{\omega} \int_0^t a(\tau) e^{-\zeta \omega (t-\tau)} \sin \omega (t-\tau) d\tau \right|$$

Schematically, D and Q for a frequency ω are shown in Figure 25 with the associated ground displacement curve. A typical horizontal displacement shock spectrum is shown in Figure 26.

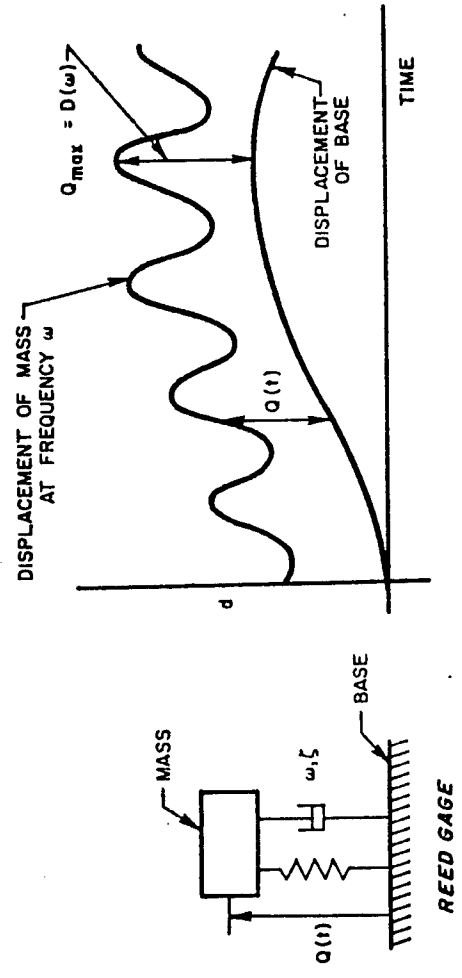


Figure 25. Response of Single Degree of Freedom System to Ground Motion

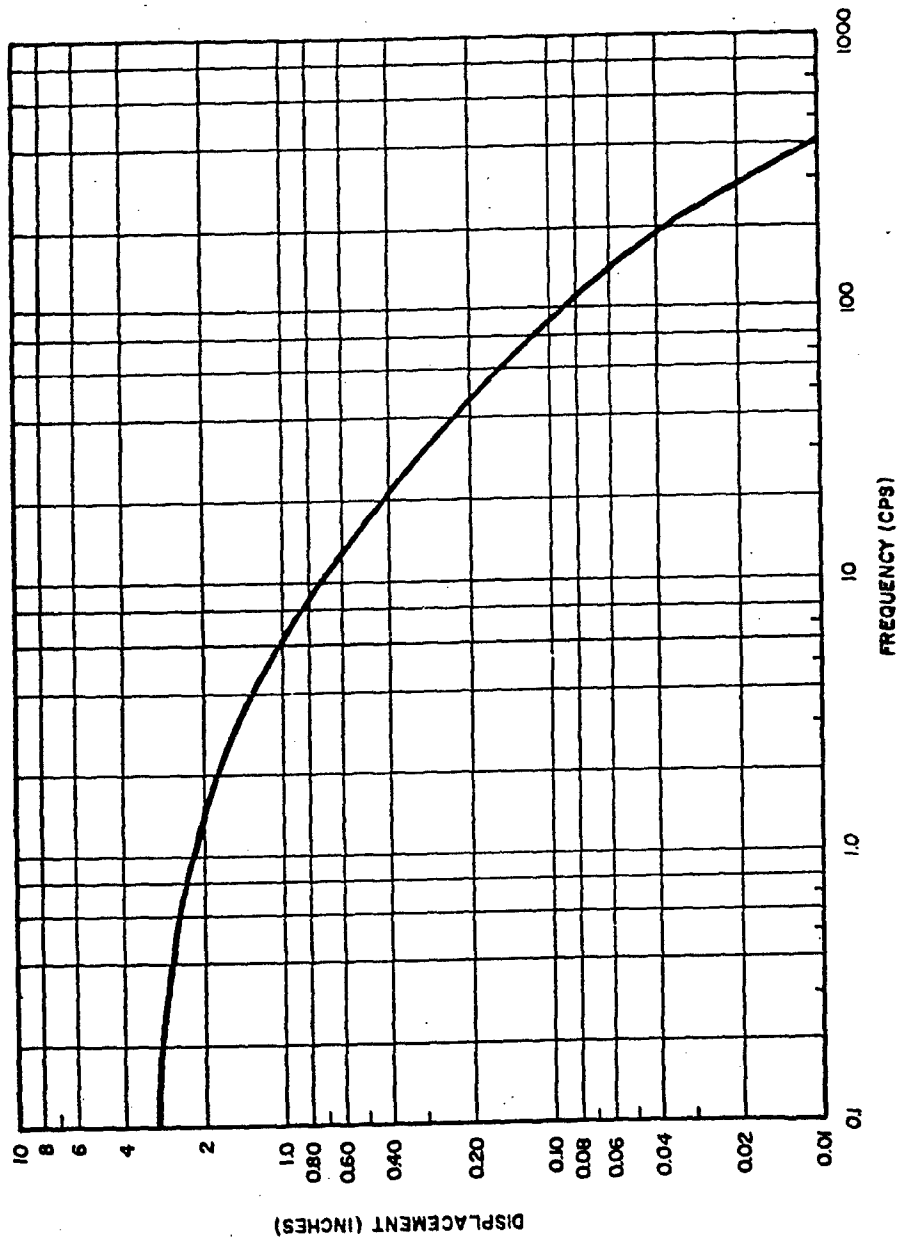


Figure 26. Horizontal Displacement Shock Spectrum

The greatest value of the response in Equation (66) would occur if all the peaks of the components occurred simultaneously and in the same phase. Since the peak value of $Q(t)$ is D , then

$$u(x) \leq \sum_n \left| \gamma_n D(\omega_n) \phi_n(x) \right|$$

Having an expression for the displacement, other quantities of interest, such as bending moment, can be obtained. The expression for bending moment is,

$$M(x) \leq \sum_n \left| \gamma_n D(\omega_n) m_n(x) \right|$$

where $m_n(x)$ is the bending moment at position x in the n th mode. These estimates of response are upper bounds; however, it has been shown by several investigators (References 23, 25, 26 and 27) that for shock inputs such as earthquake or ground shock, the estimate is not more than 15 percent conservative. The conservativeness of the response when using single pulse shock inputs is discussed in detail in Reference 25.

Such a "shock-spectra" technique of analysis is also a very valuable tool in determining the response of a missile during engine thrust build-up if the boundary conditions do not change. For example, if a missile is constrained in a launcher or if it is free-free as in the case of a space vehicle at the time of engine ignition after a coast period, an upper bound of response may be obtained by using a modal analysis if the input force (engine thrust) is represented by its "shock spectrum".

APPENDIX
 MODELS FOR THE LONGITUDINAL VIBRATIONS OF LIQUID
 PROPELLANT MISSILES

A. Equations for a Simple Cylindrical Tank

A lumped parameter model is constructed to approximate the first mode of vibration of a liquid-filled elastic tank which is considered to be a tandem part of a missile as in Figure 21. The propellant tank is shown in Figure 27. The force F in the figure is the force in the tank walls due to the action of masses above the tank under consideration. P_o is the ullage pressure in the tank. Other quantities are evident from the figure. The axial stress, σ_x , and radial stress, σ_y , in the tank wall are;

$$\sigma_x = \frac{-F}{2\pi R t} + \frac{P_o R}{2t} \tag{A. 1}$$

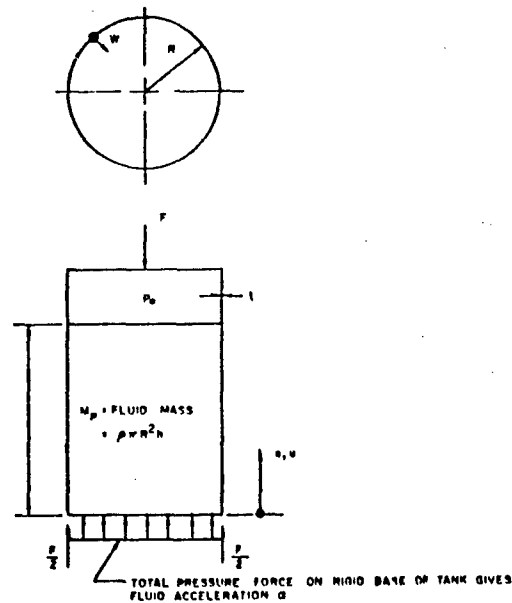


Figure 27. Propellant Tank

$$\sigma_y = \frac{P_o R}{t} + \frac{\rho a (h - x)R}{t} \quad (\text{A. 2})$$

Applying Hooke's law, the corresponding strains are;

$$\begin{aligned} \epsilon_x &= \frac{1}{E} (\sigma_x - \nu \sigma_y) \\ &= \frac{R}{Et} \left[\left(\frac{1}{2} - \nu \right) P_o - \frac{F}{2\pi R^2} - \nu \rho a (h - x) \right] \end{aligned} \quad (\text{A. 3})$$

$$\begin{aligned} \epsilon_y &= \frac{1}{E} (\sigma_y - \nu \sigma_x) \\ &= \frac{R}{Et} \left[\left(1 - \frac{\nu}{2} \right) P_o + \rho a (h - x) + \frac{\nu F}{2\pi R^2} \right] \end{aligned} \quad (\text{A. 4})$$

where;

E = Young's modulus

ν = Poisson's ratio

For tanks with a very high radius to thickness ratio, R/t , the bending deflections caused by constraints at the base of the tank can be neglected. With this assumption, the tank walls expand out into the shape of a simple truncated cone. The displacements u and w are given by kinematics as;

$$\begin{aligned} u &= \int_0^x \epsilon_x dx \\ &= \frac{R}{Et} \left[\left(\frac{1}{2} - \nu \right) P_o x - \frac{Fx}{2\pi R^2} - \nu \rho a \left(hx - \frac{x^2}{2} \right) \right] \end{aligned} \quad (\text{A. 5})$$

$$w = -R\epsilon_y$$

$$= -\frac{R^2}{Et} \left[\left(1 - \frac{\nu}{2}\right) P_o + \rho a (h - x) + \frac{\nu F}{2\pi R^2} \right] \quad (\text{A. 6})$$

In solving a longitudinal transient problem, the stresses due to the static ullage pressure, P_o , can be added separately to the dynamic stresses. Dropping these static terms, the displacement of the section of the tank at the free fluid surface relative to the base is,

$$u(h) = -\frac{R}{Et} \left[\frac{Fh}{2\pi R^2} + \nu \rho a \frac{h^2}{2} \right] \quad (\text{A. 7})$$

The total mass of the propellant and a lumped spring constant for the tank are respectively,

$$M_p = \pi R^2 h \rho \quad (\text{A. 8})$$

$$K = \frac{AE}{h} = \frac{2\pi R t E}{h} \quad (\text{A. 9})$$

The displacement of Equation (A. 7) can be written as,

$$u(h) = -\frac{F}{K} - \frac{\nu M_p}{K} a \triangleq x_1 - x_o \quad (\text{A. 10})$$

where;

x_1 = coordinate of the tank position at free surface of the liquid measured from static equilibrium.

x_o = coordinate of the tank base, measured from static equilibrium

Assume now that the fluid can be treated as a rigid body, and that its displacement is the vertical displacement of the center of gravity of the fluid which occurs when the tank walls expand from $w = 0$ to $w = w(x)$ as given by Equation (A. 6). Neglecting second order volumes, this distance (see Figure 28) is,

$$\begin{aligned} x_p - x_o &= \frac{1}{\pi R^2} \int_0^{h/2} 2\pi R w(x) dx \\ &= -\frac{3M_p}{2K} a - \frac{\nu F}{K} \end{aligned} \quad (\text{A. 11})$$

where, x_p = coordinate of fluid cg, measured from static equilibrium

Eliminating F from Equations (A. 10) and (A. 11) and noting that $a = \ddot{x}_p$, one obtains;

$$x_p - x_o = -\frac{3M_p}{2K} \ddot{x}_p + \nu \left[(x_1 - x_o) + \frac{\nu M_p}{K} \ddot{x}_p \right] \quad (\text{A. 12})$$

This equation can be rewritten using,

$$(x_1 - x_o) = (x_1 - x_p) - (x_p - x_o)$$

as,

$$M_p \ddot{x}_p + \frac{(2 - 2\nu)K}{(3 - 2\nu^2)} (x_p - x_o) - \frac{2\nu K}{(3 - 2\nu^2)} (x_1 - x_p) = 0 \quad (\text{A. 13})$$

Notice that Equation (A. 13) corresponds to Figure 29 if one takes,

$$K_1 = \left(\frac{2\nu}{3 - 2\nu^2} \right) K$$

$$K_2 = \left(\frac{2 - 2\nu}{3 - 2\nu^2} \right) K \quad (\text{A. 14})$$

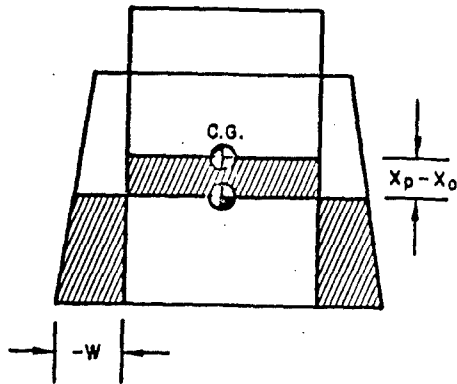


Figure 28. Displacement of Fluid due to Tank Wall Expansion

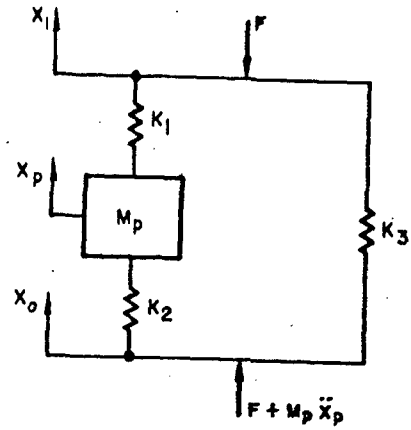


Figure 29. Longitudinal Model of Propellant Tank

The spring K_3 has been included, because neither Equation (A. 10) nor (A. 11) gives the same deflections as found in the figure if $K_3 = 0$. To find K_3 , set $\ddot{x}_p = 0$ and make the figure match the equation.

$$x_p - x_0 = -\frac{vF}{K} \quad (\text{A. 15})$$

Using Equation (A. 14) the force in spring K_2 is,

$$F_2 = \frac{-vF}{K} \left(\frac{2 - 2v}{3 - 2v^2} \right) K = -\left(\frac{2v - 2v^2}{3 - 2v^2} \right) F \quad (\text{A. 16})$$

Also, the deflection of spring K_3 , using Equation (A. 10 with $\ddot{x}_p = 0$, is

$$x_1 - x_0 = -\frac{F}{K}$$

Equilibrium of the lower bar in Figure 29 under these forces requires that,

$$\left(\frac{2v - 2v^2}{3 - 2v^2}\right) F + K_3 \frac{F}{K} = F \quad (\text{A. 17})$$

Solving for K_3 gives,

$$K_3 = \left(\frac{3 - 2v}{3 - 2v^2}\right) K \quad (\text{A. 18})$$

In Figure 21, therefore, by using Equations (A. 14) and (A. 18)

$$K_5 = \left(\frac{3 - 2v}{3 - 2v^2}\right) K$$

$$K_6 = \left(\frac{2 - 2v}{3 - 2v^2}\right) K$$

$$K_7 = \left(\frac{2v}{3 - 2v^2}\right) K$$

B. Model for a Cylindrical Tank With a Flexible Lower Bulkhead

If, instead of having a rigid base, as implied for the tank in Section A, the tank lower bulkhead has an equivalent spring constant K_{BH} , the model in Figure 29 must be modified as shown in Figure 30. It is evident that the static deflection of the liquid mass relative to the reference plane x_0 is merely that due to the flexible tank plus that due to the flexible lower bulkhead, so that the spring from the mass to the reference plane is simply these two effective springs in series, as shown. When a force F is applied to the tank skin from above, the

deflections of x_1 and x_p with respect to the reference plane are the same as if the bulkhead were rigid because no further load is carried by the bulkhead (i.e. it carries only the fluid). Thus,

$$(x_1 - x_o) = -\frac{F}{K} \quad , \quad (x_p - x_o) = -\frac{\nu F}{K} \quad (\text{A. 19})$$

as before, the new spring constants, \bar{K}_1 and \bar{K}_2 are now determined so that these deflections indeed result. From Figure 30 and Equation (A. 19) one can write,

$$(x_p - x_o) = \frac{F - \bar{K}_3 \left(\frac{F}{K}\right)}{\bar{K}_2} = -\frac{\nu F}{K}$$

from which

$$\bar{K}_3 = K - \nu \bar{K}_2 \quad (\text{A. 20})$$

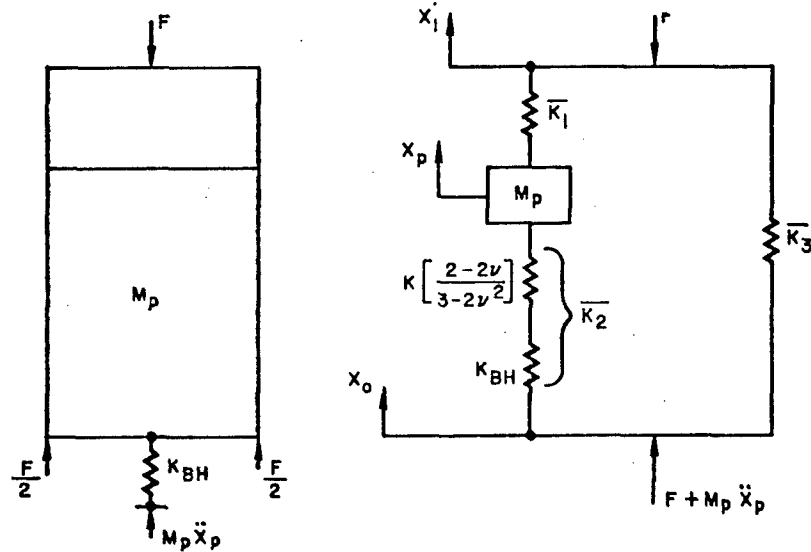


Figure 30. Longitudinal Model of Propellant Tank With Flexible Lower Bulkhead

From Figure 30, \bar{K}_2 is computed to be,

$$\bar{K}_2 = \frac{\left(\frac{2-2\nu}{3-2\nu^2}\right) K K_{BH}}{\left(\frac{2-2\nu}{3-2\nu^2}\right) K + K_{BH}}$$

Also from Figure 30 and Equation (A. 19),

$$(x_1 - x_0) \frac{-F}{\left(\frac{1}{\bar{K}_1 + \bar{K}_2}\right) + k_3} = \frac{-F}{K}$$

so that,

$$\bar{K}_1 = \frac{\bar{K}_2}{1-\nu} \tag{A. 21}$$

C. Model for a Semi-Monocoque Cylinder

If the cylinder is constructed from a skin-stringer design as shown in Figure 31 it is assumed that the stringers have negligible radial displacement but that the skin will displace both radially and longitudinally. The axial force path is either through the skin or the stringers, therefore the stringers act in parallel with the skin. The model for the skin is similar to the case in Section A., but now,

$$K_m = \frac{(AE)_{\text{skin}}}{h}$$

and the stringer spring constant is,

$$K_s = \frac{(AE)_{\text{stringer}}}{h}$$

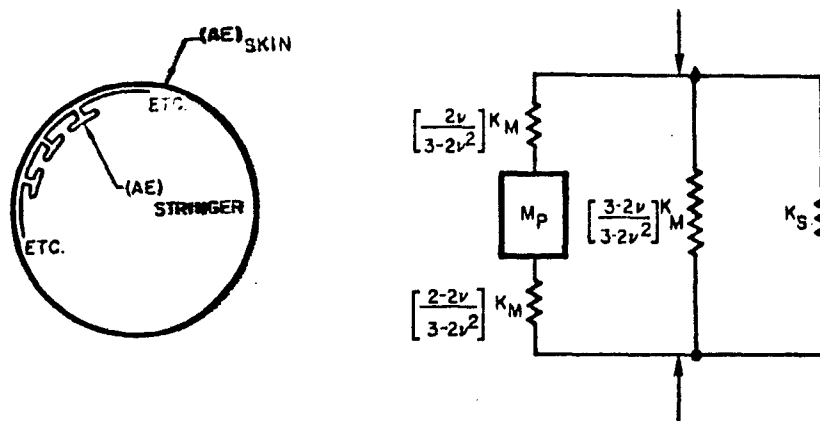


Figure 31. Section of Skin-Stringer Cylinder and Longitudinal Model

D. Model for a Semi-Monocoque Cylinder With Partially Buckled Skin

A longitudinal model of a skin-stringer propellant tank with a partially buckled skin is necessary for some of the ballistic missiles. As in the previous section it is assumed that the axial load is transmitted by the stringers, K_s , and by the effective (unbuckled) skin, K_{MB} , where the latter is,

$$K_{MB} = \left[\frac{(AE)_{skin}}{h} \right] \text{ effective}$$

The spring-mass model to represent this case is shown in Figure 32. The constants K_1^* and K_3^* are such that,

$$x_1 - x_0 = - \frac{F}{K_{MB} + K_s} \tag{A. 22}$$

and the propellant mass, M_p , deflects if a portion of the load F , say F_{MB} , that is carried by K_{MB} is transmitted by the unbuckled skin, K_M , i.e.,

$$x_p - x_o = - \frac{\nu F_{MB}}{K_M}$$

(see Equation A. 15) but,

$$\frac{F_{MB}}{K_{MB}} = \frac{F}{K_{MB} + K_s} \quad , \quad \text{where } K_M = \frac{(AE)_{skin}}{h}$$

therefore,

$$x_p - x_o = - \frac{\nu F K_{MB}}{K_M (K_{MB} + K_s)} \quad (A. 23)$$

Equations (A. 22) and (A. 23) are the constraints to be satisfied.

Assuming, as before, that $\ddot{x}_p = 0$ then from Figure 32 and Equation (A. 22),

$$-\frac{F}{(x_1 - x_o)} = \frac{K_1^* \left(\frac{2 - 2\nu}{3 - 2\nu^2} \right) K_M}{K_1^* + \left(\frac{2 - 2\nu}{3 - 2\nu^2} \right) K_M} + K_3^* + K_s = K_{MB} + K_s$$

therefore,

$$K_{MB} = K_3^* + \frac{\left(\frac{2 - 2\nu}{3 - 2\nu^2} \right) K_M K_1^*}{\left(\frac{2 - 2\nu}{3 - 2\nu^2} \right) K_M + K_1^*} \quad (A. 24)$$

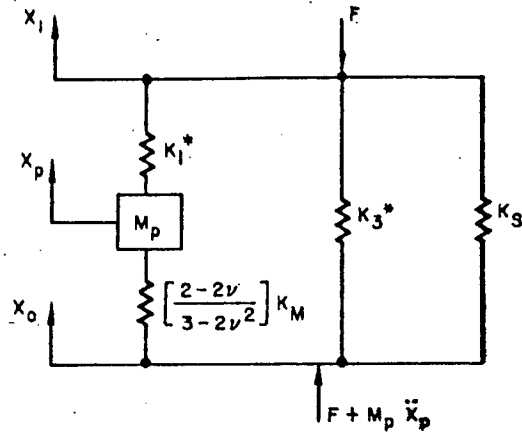


Figure 32. Longitudinal Model of Semi-Monocoque Cylinder with Partially Buckled Skin

From Figure 32 and Equation (A. 23),

$$-\frac{F}{(x_p - x_0)} = \frac{\left(\frac{2-2\nu}{3-2\nu^2}\right) K_M}{\left(1 - \frac{K_3^* + K_S}{K_{MB} + K_S}\right)} = \frac{K_M (K_{MB} + K_S)}{\nu K_{MB}}$$

therefore,

$$K_3^* = \left(\frac{3-2\nu}{3-2\nu^2}\right) K_{MB} \quad (\text{A. 25})$$

Substituting Equation (A. 25) into Equation (A. 24) gives,

$$K_1^* = \frac{\left(\frac{2-2\nu}{3-2\nu^2}\right) \nu K_M K_{MB}}{K_M - \nu K_{MB}} \quad (\text{A. 26})$$

The foregoing derived spring constants for Figure 32 are shown in Figure 33.

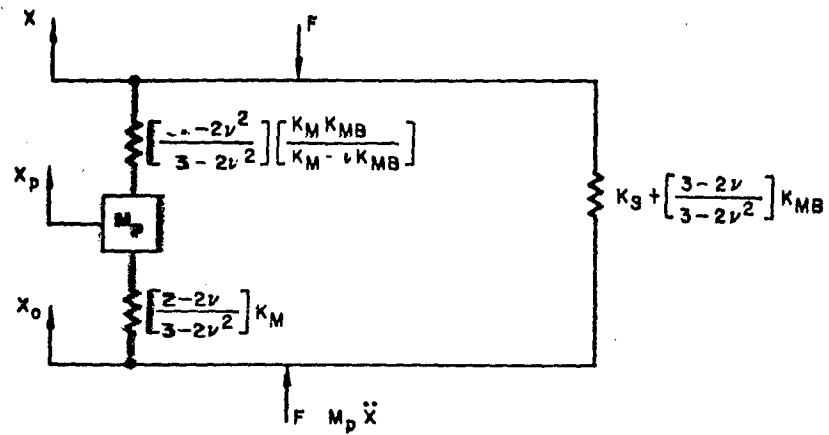


Figure 33. Simplified Model of Figure 32

REFERENCES

1. A. P. Goldberg and J. D. Wood. "Dynamic Loads in the Atlas-Able 5 during Transonic Buffeting," STL/TM-60-0000-19075, August 22, 1960.
2. A. P. Goldberg and R. H. Adams. "Mercury-Atlas Buffeting Loads at Transonic and Low Supersonic Speeds," STL/TR-60-0000-AS431, November 28, 1960.
3. J. D. Wood. "Response of Minuteman Missile due to Microseisms," STL memo GM 59.7520.1-249, December 9, 1959.
4. M. V. Barton. "Generalized Missile Dynamic Analysis, I-Development and Application," STL report EM 8-7, April 7, 1958.
5. D. Young. "Generalized Missile Dynamic Analysis, II-Equations of Motion," STL report EM 8-8, April 7, 1958.
6. J. W. Miles and D. Young. "Generalized Missile Dynamic Analysis, III-Aerodynamics," STL report EM 8-9, April 7, 1958.
7. J. W. Miles and D. Young. "Generalized Missile Dynamic Analysis, IV-Sloshing," STL report EM 8-10, April 7, 1958.
8. J. Fowler. "Generalized Missile Dynamic Analysis, V-Calculation of Bending Modes," STL report EM 8-16, April 7, 1958.
9. D. C. Martin. "Generalized Missile Dynamic Analysis, VI-Control System Equations," STL report EM 8-14, April 7, 1958.
10. J. A. Brooks. "Generalized Missile Dynamic Analysis, VII-Programming," STL report EM 8-15, April 7, 1958.
11. H. E. Lindberg and H. L. Gamage. "Orthogonality Relations for Branched Timoshenko Beams including Axial Acceleration and Attached Spring - Masses," GM 60-7520.1-237a, 30 June 1960.
12. H. E. Lindberg and H. L. Gamage. "In-Flight Dynamics of a Flexible Missile," STL/TR-60-0000-00083a, EM 10-4A, October 1960.
13. S. Timoshenko. Vibration Problems in Engineering, D. Van Nostrand, Co., Inc. Princeton, N.J.

14. R. M. Cooper. "Dynamics of Liquids in Moving Containers," ARS J., 30, No. 8 (1960)
15. H. E. Lindberg. "Effect of Support Conditions and Shaker Arrangements in Beam Vibration Testing," 4th Symposium on Ballistic Missiles and Space Technology, University of California, Los Angeles, 1959, or STL report GM-TR-0165-00533, EM 8-24, December 16, 1958.
16. R. L. Bisplinghoff, H. Ashley, and R. L. Halfman, Aeroelasticity, Addison-Wesley Press, Reading, Mass., 1955.
17. Y. C. Fung, The Theory of Aeroelasticity, John Wiley and Sons, New York, 1955.
18. Y. C. Fung. "Fluctuating Lift and Drag Acting on a Cylinder in a Flow at Supercritical Reynolds Numbers," Bulletin, 26th Shock and Vibration Symposium, Dept. of Defense, 1958, or STL report GM-TR-0165-00343, EM 8-5, 7 May 1958.
19. A. A. Ebra. "Wind Induced Oscillations of the Titan Missile," WDD-M MI-59-7, Martin Company, Denver 1, Colorado, March 1959.
20. D. A. Buell, and G. C. Kenyon. "The Wind-Induced Loads on a Dynamically Scaled Model of a Large Missile in Launching Position," NASA TM X-109, Ames Research Center, Moffett Field, California.
21. M. V. Barton and W. T. Thomson. "The Response of Mechanical Systems to Random Excitation," Journal of Applied Mechanics, vol. 24, No. 2, June 1957, p. 248
22. H. L. Gamage. "Dynamic Response of the Titan Missile due to Wind," STL/TN-59-0000-09354, December 7, 1959.
23. M. V. Barton, Shock and Structural Response, papers presented at a colloquium on shock and structural response at the Annual Meeting of the ASME, November 30, 1960. The American Society of Mechanical Engineers, New York.
24. M. V. Barton. "Ground Shock Measurements and Structural Response," EM 7-18, GM-TR-293, December 11, 1957.
25. Y. C. Fung and M. V. Barton. "Some Shock Spectra Characteristics and Uses," Journal of Applied Mechanics, September 1958, Vol 25, 3 p. 365

6. G. W. Housner. "Spectrum Intensities of Strong-Motion Earthquakes," Proc. of the Symposium on Earthquake and Blast Effects in Structures, University of California, Los Angeles, 1952.
27. J. D. Wood. "Factors affecting the Response of Missiles excited by Ground Shock," Shock, Vibration and Associated Environments, Part III, Bulletin No. 28 September 1960, Office of the Secretary of Defense, Washington, D. C., or STL/TN-60-0000 09031, February 5, 1960.
28. Ballistic Missile and Space Vehicle Systems, Chapter 12, by J. G. Berry, H. E. Lindberg, and J. D. Wood to be published by John Wiley and Sons, Inc., New York - London, 1961.

UNCLASSIFIED

Space Technology Laboratories, Inc., P. O. Box 95001, Los Angeles 45, California
SURVEY ON MISSILE STRUCTURAL DYNAMICS,
by John D. Wood, 1 June 1961, 88 pages
(7102-0041-NU-000, EM 11-11; BSD-TN-61-42)
(Contract AF 04(647)-619) Unclassified report

This report is a survey of the more common types of structural dynamics problems in association with ballistic missiles. Special attention is given to the effects of subsystem interaction on dynamic response of the missile and vice versa. A few technically important examples are treated in some detail. The purpose of these examples is twofold: first, they illustrate various techniques used in dynamics analysis and second, they record some of the details of mathematical models which are frequently used to solve missile dynamics response problems. Some of the sections of this report are found in the references, but are repeated here to provide the reader with a fairly complete picture of the more common types of missile structural dynamics problems.

UNCLASSIFIED

UNCLASSIFIED

Space Technology Laboratories, Inc., P. O. Box 95001, Los Angeles 45, California
SURVEY ON MISSILE STRUCTURAL DYNAMICS,
by John D. Wood, 1 June 1961, 88 pages
(7102-0041-NU-000, EM 11-11; BSD-TN-61-42)
(Contract AF 04(647)-619) Unclassified report

This report is a survey of the more common types of structural dynamics problems in association with ballistic missiles. Special attention is given to the effects of subsystem interaction on dynamic response of the missile and vice versa. A few technically important examples are treated in some detail. The purpose of these examples is twofold: first, they illustrate various techniques used in dynamics analysis and second, they record some of the details of mathematical models which are frequently used to solve missile dynamics response problems. Some of the sections of this report are found in the references, but are repeated here to provide the reader with a fairly complete picture of the more common types of missile structural dynamics problems.

UNCLASSIFIED

UNCLASSIFIED

Space Technology Laboratories, Inc., P. O. Box 95001, Los Angeles 45, California
SURVEY ON MISSILE STRUCTURAL DYNAMICS,
by John D. Wood, 1 June 1961, 88 pages
(7102-0041-NU-000, EM 11-11; BSD-TN-61-42)
(Contract AF 04(647)-619) Unclassified report

This report is a survey of the more common types of structural dynamics problems in association with ballistic missiles. Special attention is given to the effects of subsystem interaction on dynamic response of the missile and vice versa. A few technically important examples are treated in some detail. The purpose of these examples is twofold: first, they illustrate various techniques used in dynamics analysis and second, they record some of the details of mathematical models which are frequently used to solve missile dynamics response problems. Some of the sections of this report are found in the references, but are repeated here to provide the reader with a fairly complete picture of the more common types of missile structural dynamics problems.

UNCLASSIFIED

UNCLASSIFIED

Space Technology Laboratories, Inc., P. O. Box 95001, Los Angeles 45, California
SURVEY ON MISSILE STRUCTURAL DYNAMICS,
by John D. Wood, 1 June 1961, 88 pages
(7102-0041-NU-000, EM 11-11; BSD-TN-61-42)
(Contract AF 04(647)-619) Unclassified report

This report is a survey of the more common types of structural dynamics problems in association with ballistic missiles. Special attention is given to the effects of subsystem interaction on dynamic response of the missile and vice versa. A few technically important examples are treated in some detail. The purpose of these examples is twofold: first, they illustrate various techniques used in dynamics analysis and second, they record some of the details of mathematical models which are frequently used to solve missile dynamics response problems. Some of the sections of this report are found in the references, but are repeated here to provide the reader with a fairly complete picture of the more common types of missile structural dynamics problems.

UNCLASSIFIED

UNCLASSIFIED

Space Technology Laboratories, Inc., P. O. Box
95001, Los Angeles 45, California
SURVEY ON MISSILE STRUCTURAL DYNAMICS,
by John D. Wood, 1 June 1961, 88 pages
(7102-0041-NU-000, EM 11-11; BSD-TN-61-42)
(Contract AF 04(647)-619) Unclassified report

This report is a survey of the more common types of structural dynamics problems in association with ballistic missiles. Special attention is given to the effects of subsystem interaction on dynamic response of the missile and vice versa. A few technically important examples are treated in some detail. The purpose of these examples is twofold; first, they illustrate various techniques used in dynamics analyses and second, they record some of the details of mathematical models which are frequently used to solve missile dynamics response problems. Some of the sections of this report are found in the references, but are repeated here to provide the reader with a fairly complete picture of the more common types of missile structural dynamics problems.

UNCLASSIFIED

UNCLASSIFIED

Space Technology Laboratories, Inc., P. O. Box
95001, Los Angeles 45, California
SURVEY ON MISSILE STRUCTURAL DYNAMICS,
by John D. Wood, 1 June 1961, 88 pages
(7102-0041-NU-000, EM 11-11; BSD-TN-61-42)
(Contract AF 04(647)-619) Unclassified report

This report is a survey of the more common types of structural dynamics problems in association with ballistic missiles. Special attention is given to the effects of subsystem interaction on dynamic response of the missile and vice versa. A few technically important examples are treated in some detail. The purpose of these examples is twofold; first, they illustrate various techniques used in dynamics analyses and second, they record some of the details of mathematical models which are frequently used to solve missile dynamics response problems. Some of the sections of this report are found in the references, but are repeated here to provide the reader with a fairly complete picture of the more common types of missile structural dynamics problems.

UNCLASSIFIED

UNCLASSIFIED

Space Technology Laboratories, Inc., P. O. Box
95001, Los Angeles 45, California
SURVEY ON MISSILE STRUCTURAL DYNAMICS,
by John D. Wood, 1 June 1961, 88 pages
(7102-0041-NU-000, EM 11-11; BSD-TN-61-42)
(Contract AF 04(647)-619) Unclassified report

This report is a survey of the more common types of structural dynamics problems in association with ballistic missiles. Special attention is given to the effects of subsystem interaction on dynamic response of the missile and vice versa. A few technically important examples are treated in some detail. The purpose of these examples is twofold; first, they illustrate various techniques used in dynamics analyses and second, they record some of the details of mathematical models which are frequently used to solve missile dynamics response problems. Some of the sections of this report are found in the references, but are repeated here to provide the reader with a fairly complete picture of the more common types of missile structural dynamics problems.

UNCLASSIFIED

UNCLASSIFIED

Space Technology Laboratories, Inc., P. O. Box
95001, Los Angeles 45, California
SURVEY ON MISSILE STRUCTURAL DYNAMICS,
by John D. Wood, 1 June 1961, 88 pages
(7102-0041-NU-000, EM 11-11; BSD-TN-61-42)
(Contract AF 04(647)-619) Unclassified report

This report is a survey of the more common types of structural dynamics problems in association with ballistic missiles. Special attention is given to the effects of subsystem interaction on dynamic response of the missile and vice versa. A few technically important examples are treated in some detail. The purpose of these examples is twofold; first, they illustrate various techniques used in dynamics analyses and second, they record some of the details of mathematical models which are frequently used to solve missile dynamics response problems. Some of the sections of this report are found in the references, but are repeated here to provide the reader with a fairly complete picture of the more common types of missile structural dynamics problems.

UNCLASSIFIED